Numerical implementation of pseudo-spectral method in self-consistent mean field theory for discrete polymer chains

Cite as: J. Chem. Phys. **150**, 234901 (2019); https://doi.org/10.1063/1.5094227
Submitted: 28 February 2019 . Accepted: 28 May 2019 . Published Online: 18 June 2019

So Jung Park, Daeseong Yong, Yeongyoon Kim, and Jaeup U. Kim

The Journal of Chemical Physics ARTICLE scitation.org/journal/jcp

Numerical implementation of pseudo-spectral method in self-consistent mean field theory for discrete polymer chains

Cite as: J. Chem. Phys. 150, 234901 (2019); doi: 10.1063/1.5094227
Submitted: 28 February 2019 • Accepted: 28 May 2019 •
Published Online: 18 June 2019

So Jung Park,[1] Daeseong Yong,[1] Yeongyoon Kim,[2] and Jaeup U. Kim[1,a)]

AFFILIATIONS

[1] Department of Physics, School of Natural Science, Ulsan National Institute of Science and Technology (UNIST), Ulsan 44919, South Korea
[2] School of Polymer Science and Engineering, Chonnam National University, Gwangju 61186, South Korea

[a)] **Electronic mail:** jukim@unist.ac.kr

ABSTRACT

In the standard self-consistent field theory (SCFT), a polymer chain is modeled as an infinitely flexible Gaussian chain, and the partition function is calculated by solving a differential equation in the form of a modified diffusion equation. The Gaussian chain assumption makes the standard SCFT inappropriate for modeling of short polymers, and the discrete chain SCFT in which the partition function is obtained through recursive integrals has recently been suggested as an alternative method. However, the shape of the partition function integral makes this method much slower than the standard SCFT when calculated in the real space. In this paper, we implement the pseudospectral method for the discrete chain SCFT adopting the bead-spring or freely jointed chain (FJC) model, and a few issues such as the accurate discretization of the FJC bond function are settled in this process. With the adoption of the pseudospectral method, our calculation becomes as fast as that of the standard SCFT. The integral equation introduces a new boundary condition, the neutral boundary, which is not available in the standard SCFT solving the differential equation. This interesting physical situation is combined with the finite-range interaction model for the study of symmetric block copolymers within thin films. We find that the surface-perpendicular block copolymer lamellar phase becomes preferable to the surface-parallel one when both the top and bottom surfaces are neutral.

I. INTRODUCTION

Polymeric materials have a wide range of scientific and technological applications especially in the field of nanoscience.[1–4] For example, in the design of well-arranged nanostructures, block copolymers are popular for the control of various material properties because they can phase-separate and self-assemble into periodic structures on nanoscale due to the connectivity and incompatibility of the blocks.[5–9] Since polymers consist of a large number of monomers which are numerically intractable in a deterministic way, in the theoretical study of polymers, equilibrium behavior of a polymeric system is described by a statistical approach, and coarse-graining procedure is usually required in the modeling of real polymer chains.

Many monomers are connected by chemical bonds in a polymer chain, and one such example is shown in Fig. 1 where each monomer in a linear polystyrene (PS) chain is represented by a small blue bead. In a mesoscopic description of a polymer chain, modeling of each bead is not necessary due to the universality established by earlier polymer theories.[10] In this regard, as shown in Fig. 1, a few beads are treated as a statistical segment, and the property of the polymers is matched by controlling the property of segments and bonds connecting them. Because of this, the theory of polymer physics has been developed into a special direction. First-principles calculation,[11–13] molecular dynamics (MD) simulation,[14–17] and Monte Carlo (MC) simulation[18,19] are still useful theoretical tools as in other fields, but a statistical mechanical tool known as the self-consistent field

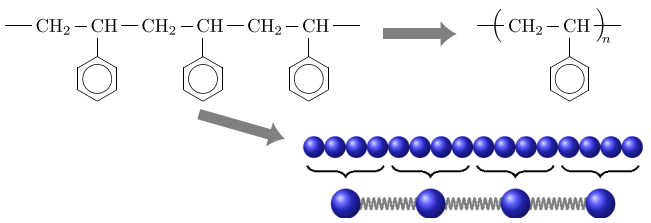

FIG. 1. Example of polymer abstraction and segment modeling of a linear PS chain with *n* styrene units. Each small blue bead represents one PS monomer. The collection of a few monomer units forms a coarse-grained segment, and the linear polymer chain is modeled by many segments connected by bonds. The coarse-grained segment and bond represent the microscopic degree of freedom of the polymer chain.

theory (SCFT)[6–8,20–23] has been established as a powerful alternative approach.

The SCFT was developed to predict the statistical behavior of a polymer system by converting a particle-based statistical description of polymers into a field-based one. In this approach, many body interactions between segments are replaced by the external potential field which is determined by the polymer density distribution, and free energy can be calculated along with the self-consistently determined potential field. This mean field approximation makes SCFT a suitable tool to simulate a large-scale system which is computationally demanding in a particle-based simulation, and the computational advantage makes it possible to successfully obtain the block copolymer phase diagram.[6,8,21,24,25]

Many SCFT frameworks have been developed so far, but the most widely used one is the Gaussian chain model,[7,8,21] which approximates a long polymer as a continuous elastic chain represented by a smooth curve in space. One reason for the popularity of this model is its simple formulation in the numerical calculation. In this formulation of SCFT, the partition function calculation reduces to solving a differential equation in the form of a modified diffusion equation. For the purpose of distinction, we will call this method the standard SCFT in this paper. Because the Gaussian chain model assumes that polymers are infinitely flexible, the standard SCFT is appropriate for the modeling of long polymers, and there is a limitation that it is only applicable to high molecular weight polymers whose average end-to-end length is much shorter than its contour length along the backbone.

Polymers with low molecular weights are one of the promising materials in recent nanoscience. For example, for the creation of sub-10 nm nanostructure, diblock copolymers with high Flory-Huggins interaction parameter χ and low polymerization index N have been widely studied.[26–28] However, the above discussion implies that when the standard SCFT is applied to the calculation of the mean field statistics of short polymer chains, it may sometimes produce unphysical results.

There is another limitation of the Gaussian chain model. It fails to explain some physical properties emerging from the discreteness of chains or physical phenomena originated from the atomistic scales. For example, the statistical mechanics of ideal polymer chains next to a hard wall and the effective surface tension due to entropic origin have been known to be difficult to calculate by using the Gaussian chain model[29–31] because it is plagued by unphysical effects such as the diverging entropy loss near the hard wall. These limitations require alternative chain modeling which can be incorporated with the SCFT for the investigation of statistical mechanics of discrete short polymer chains.

Alternative polymer models which may resolve these issues are indeed available. For example, lattice SCFT adopting random walks with fixed direction and length has been available from the earlier development of the SCFT,[32–35] but due to its limitation in accuracy and speed, the standard SCFT has become more popular and the lattice SCFT is now used in limited situations only. An SCFT method accounting for the stiffness of chains by the wormlike chain model has been suggested and recently used to solve a few problems.[31,36,37] However, the dimensionality of the differential equation increases when moving away from the Gaussian chain model, and the computational demands increase dramatically for the three-dimensional problems.

Recently, there have been some attempts to apply the SCFT to discrete polymer chains consisting of a finite number of segments connected together by the freely jointed or Hookian-spring bonds. In this discrete chain formulation, the partition functions are calculated through iterative integral equations rather than solving the diffusion equation as in the standard SCFT. For its distinction from the standard SCFT, we will call this method discrete chain SCFT in this paper. The fundamental idea of the discrete chain SCFT is that the chain propagation is described as a stochastic process, and the partition function of each segment is recursively built up from an integral representation of the probability distribution known as the Chapman-Kolmogorov equation.[38] In some polymer physics textbooks,[21,39,40] the integral equation approach using the discrete chain model is often presented as an intermediate step for the introduction of the continuous Gaussian chain model because the discrete chain is easier to visualize and its convergence to the Gaussian chain is intuitive from the central limit theorem. In continuous limit, the integral equations for calculating the discrete chain statistics can be reduced to a linear partial differential equation which we will introduce later.

Even though the discrete chain formulation has been known from the early stage of polymer field theory, numerical implementation of the integral equation approach to the analysis of complex polymeric systems has become popular only in recent years. In 2009, Matsen, Kim, and Likhtman published a paper performing the numerical calculation of the freely jointed chain (FJC) partition function near a neutral wall.[30] In this approach, the partition function of the polymer segments is calculated by one-dimensional spatial integrals accounting for the probability change from one segment to another. Later works extend this method for the analysis of chain end distribution of short incompressible polymers next to a surface.[41–43] Romeis *et al.* also adopted a similar methodology in the SCFT calculation of a brush system.[44] They used the off-lattice model for FJC, and their results were compared with the MD simulation data.

Even though the above papers successfully implemented the integral equation approach of the partition function calculation, the formulations are limited to one-dimensional systems after assuming translational invariance in the lateral direction. For a general problem with three-dimensional complexity, however, accurate calculation of the partition function in real space becomes extremely

costly. As will be discussed in more detail in Sec. IV, three-dimensional calculation of the discrete chain SCFT is inevitably slower than the standard SCFT.

Recently, Matsen demonstrated that this issue can be resolved by using the spectral method where all calculations are performed in Fourier space with symmetrized basis functions.[45] In his paper, the free energies of complex block copolymer morphologies are calculated using efficient numerical implementation of the discrete chain SCFT adopting the FJC model. As a result, the full phase diagram of diblock copolymers with low molecular weights is obtained, and he found a noticeable upward shift of the order-disorder transition χN after assuming finite-range interaction between segments. This study proves that the discrete chain SCFT can be equally efficient to the standard SCFT adopting the Gaussian chain model when implementing the full-spectral approach. This efficiency comes from the symmetry in ordered periodic morphologies which reduces the number of required Fourier coefficients, but such a symmetry may not be present in many polymer science problems. In addition, there is a disadvantage in conducting some calculations in Fourier space. Simple scalar multiplications in real space would become a matrix multiplication which is computationally costly to perform in Fourier space.

This complication can be avoided by using a pseudospectral strategy which allows flexible switch between Fourier space and real space, and this numerical method is known to be less restrictive and more versatile compared to the full spectral method. Adoption of the pseudospectral method for solving the recursive integral equations of the partial partition function has been suggested earlier by Fredrickson,[21] and Matsen also mentioned the possibility of the pseudospectral method for the fast calculation of the discrete chain SCFT.[45] However, the actual implementation of the pseudospectral method in the calculation of the discrete chain SCFT has not been reported yet.

In this paper, we present a generic theory of the discrete polymer chain SCFT in a form ready for the optimal implementation of the pseudospectral method. There are some unexpected issues one inevitably faces in the implementation of the pseudospectral algorithm, and the details will be discussed later. After the successful implementation, we test various properties of short polymer chains with the finite number of segments. In addition, to test the practicality of the algorithm, the fundamental problem of block copolymer morphology confined between two walls is investigated using this approach.

The outline of this paper is as follows. In Sec. II, the basic idea of the discrete chain SCFT is introduced. We then present its algebraic formulation and the adoption of the pseudospectral method in Secs. III and IV. In Sec. V, the details of the implementation of the pseudospectral method are explained along with the treatment of a neutral wall in this formalism. In Sec. VI, the results of our discrete chain SCFT calculation including the block copolymer morphology confined by neutral walls are presented. Finally, we conclude in Sec. VII with a brief discussion on the advantage of this theoretical method.

II. BACKGROUND

The most popular version of the SCFT nowadays is based on the Gaussian chain model. It is typical to introduce the Gaussian chain model from discrete N segments as seen in Fig. 1, and by taking the long chain limit ($N \to \infty$), the chain becomes infinitely flexible. In this standard SCFT formalism, the segment position along the backbone of the polymer is specified by a continuous parameter $s \in [0, 1]$ [see Fig. 2(a)], and this model allows the use of modified diffusion equation for the calculation of the partition function which is required for the prediction of the statistical behavior of the polymer system.

The partial partition function of sN segments starting from the $s = 0$ chain end can be written as $q(\mathbf{r}, s)$, where $\mathbf{r}$ is the sNth segment position, and it satisfies the following modified diffusion equation:

$$\frac{\partial}{\partial s} q(\mathbf{r}, s) = \left(\frac{a^2 N}{6} \nabla^2 - w(\mathbf{r}) \right) q(\mathbf{r}, s), \tag{1}$$

where a is the statistical segment length and $w(\mathbf{r})$ is the self-consistently determined mean potential field acting on the segment at position $\mathbf{r}$.[8,21] The complementary partial partition function of $(1 - s)N$ segments starting from the $s = 1$ chain end, $q^{\dagger}(\mathbf{r}, s)$, satisfies the same modified diffusion Eq. (1) with the left-hand side multiplied by -1. Using these two partial partition functions, mean field quantities such as the total partition function of the chain and the polymer density distribution can be calculated. The mean field free energy of the system is found after the self-consistent solution is obtained.

It is obvious that a real polymer is not infinitely flexible, and the Gaussian chain model inevitably fails at a small scale. As explained in the Introduction, this problem becomes more significant for short polymer chains, and we need to recheck the fundamentals of the polymer statistics calculation to find a valid alternative method.

One suggestion is to directly solve the integral equations of partition functions which utilizes the theory of the Markovian stochastic process.[38] This approach retains the discreteness of chain by assuming a finite number of segments, and as shown in Fig. 2(c), the segment positions along the polymer backbone are now specified by N discrete points of $s = n\Delta s$ ($n \in \{0, 1, \ldots, N-1\}$),

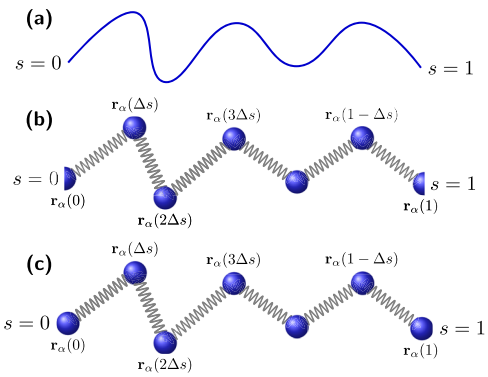

FIG. 2. The polymer chain parameterization of the (a) Gaussian chain model, (b) N bond model, and (c) $N - 1$ bond model. For the Gaussian chain model, the curve $\mathbf{r}_\alpha(s)$ is defined at all s in [0, 1], but the function is defined only at discrete points with intervals $\Delta s \equiv 1/N$ and $\Delta s \equiv 1/(N - 1)$ for the cases of the N bond model and the $N - 1$ bond model, respectively.

where $\Delta s \equiv 1/(N-1)$. Its fundamental idea is that the probability density to observe the $(s+\Delta s)N$th segment at position $\mathbf{r}$ can be built up by means of a Chapman-Kolmogorov equation when the probability density distribution of the sNth segment is already known.[21,30,39,40]

For a noninteracting chain, random step propagation of the chain suggests that the partial partition function $q(\mathbf{r}, s+\Delta s)$ can be recursively obtained from the distribution of the sNth partial partition function, $q(\mathbf{r}, s)$,

$$q(\mathbf{r}, s+\Delta s) = \int d\mathbf{R}\, g(\mathbf{R}; \mathbf{r}-\mathbf{R}) q(\mathbf{r}-\mathbf{R}, s), \tag{2}$$

where the bond function $g(\mathbf{R}; \mathbf{r}-\mathbf{R})$ represents the conditional probability density that the bond vector from the sNth segment located at position $\mathbf{r}-\mathbf{R}$ to the $(s+\Delta s)N$th segment assumes a displacement vector of $\mathbf{R}$. The partition function $q(\mathbf{r}, s)$ can be built up recursively for all segment points $s = n\Delta s$ starting from $n = 0$.

In the absence of external fields, the random walking nature of the chain shows the Markov process, and the probability distribution of the bond $g(\mathbf{R}; \mathbf{r}-\mathbf{R})$ becomes independent of the starting position which allows us to use one variable function $g(\mathbf{R})$ throughout this paper. In the theory of statistical mechanics, statistical weight of each segment is closely related with its probability density, and thus Eq. (2) corresponds to the Chapman–Kolmogorov equation in the theory of the stochastic process. Considering that Eq. (1) is the differential form of the Chapman–Kolmogorov equation, the relation of the above equations becomes easier to understand. The solution of the partition functions obtained by this integral method reduces to the solution of the modified diffusion equations without field in the limit Δs goes to 0.

However, considering that the integral approach helps us to reveal the property of discrete chains, it is an attractive idea to remain in the discrete chain model especially when we are interested in the behavior of short polymer chains. Previous papers adopting this model have directly borrowed the integral equations, but in Sec. III, we will rigorously derive the formalism of the discrete chain SCFT in an integral form, starting from the fundamental definition of the partition function and free energy. In doing so, whenever we have a choice, we will adopt a method which is optimized for the numerical implementation and which can easily visualize its convergence to the standard SCFT.

III. DISCRETE CHAIN SCFT

A. Algebraic formulation

This subsection presents the discrete chain SCFT formulation of a sample system with an incompressible melt of AB block copolymers. The system is composed of n_p symmetric AB block copolymer chains with A fraction $f = 0.5$ and total segment number N. We first present the coarse-grained chain model with the most intuitive choice, and then we will move onto a different model. As depicted in Fig. 3(a), the AB block copolymer chain consists of many A and B types of monomers.

In the process of chain modeling, a few monomers are coarse-grained to form a segment; in the figure, by combining four monomers in one segment, $N/2$ A segments and $N/2$ B segments are constructed. The random walking nature of the polymer chain is embedded in the bond connecting the neighboring segments, and the property of the bond depends on the actual architecture of the chain and the scale of coarse-graining. By choosing an even number of N, each segment is either A or B type, and this modeling looks very natural for the representation of a discrete chain of N segments. In the absence of field, the natural end-to-end distance of the chain becomes $R_0 = a(N-1)^{1/2}$, not the well-known expression $aN^{1/2}$, since the number of bonds is actually $N-1$.

For the convenience of mathematical formulation, however, we now present another possible polymer chain model which may look unnatural at first glance for those who are not accustomed to it. In this model, when combining monomers to form segments, we start the process by creating a half-segment as shown in Fig. 3(b) and label it as the 0th segment for convenience. All the subsequent segments are full-segments except the last (Nth) one which is again a half-segment. The total number of points is now $N+1$, but because two of them are half-segments, we formally count N segments. One advantage of this modeling is that since the bond and segment numbers are the same, it is not required to modify the end-to-end distance expression $R_0 = aN^{1/2}$ even for low molecular weight polymers with small N. For future distinction,we will use the term

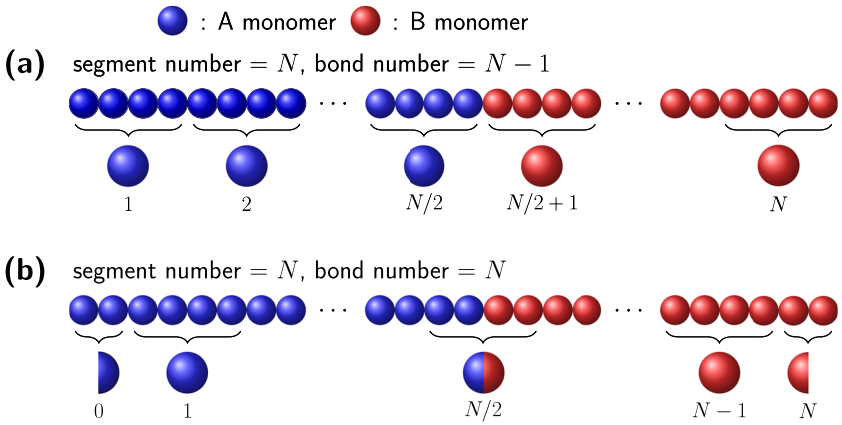

FIG. 3. (a) Symmetric ($f = 0.5$) diblock copolymer with N beads and $N-1$ bonds. (b) Symmetric diblock copolymer with N beads and N bonds.

"$N-1$ bond model" and "N bond model" for Figs. 3(a) and 3(b), respectively.

Even though the former choice seems to be more natural, let us start our algebraic formulation from the N bond model. It is partially because the equations become simpler in this model, and its modification to the $N-1$ bond model is a trivial task as explained at the end of this section. For the recursive equation of the N bond model, calculation of the partial partition function becomes multiple applications of a single evolution step without any exception because any chain fragment in the intermediate step has two half-segment ends unlike the $N-1$ bond model.

The segment positions of the αth polymer chain can be represented by the function $\mathbf{r}_\alpha(s)$, as shown in Fig. 2(b). In the standard SCFT, $\mathbf{r}_\alpha(s)$ is a continuous function, but for the discrete chain, its values at $N+1$ discrete points of $s = n\Delta s$ ($n \in \{0, 1, \ldots, N\}$ and $\Delta s \equiv 1/N$) are only meaningful, and we assume that the polymer mass is concentrated at these positions. Even though each segment has a volume ρ_0^{-1}, it can be treated as a pointlike object for the density calculation.

Considering that the 0th and Nth segments are half-segments, the spatial densities of A and B type segments in the αth chain are given as

$$\hat{\phi}_{\alpha,\mathrm{A}}(\mathbf{r}) = \frac{1}{\rho_0} \sum_{s\in\{0,\ldots,f\}}{}' \delta(\mathbf{r}-\mathbf{r}_\alpha(s)), \tag{3a}$$

$$\hat{\phi}_{\alpha,\mathrm{B}}(\mathbf{r}) = \frac{1}{\rho_0} \sum_{s\in\{f,\ldots,1\}}{}' \delta(\mathbf{r}-\mathbf{r}_\alpha(s)), \tag{3b}$$

$$\sum_{s\in\{t,\ldots,u\}}{}' f(s) \equiv \frac{f(t)}{2} + f(t+\Delta s) + \cdots + f(u-\Delta s) + \frac{f(u)}{2}, \tag{3c}$$

where we assume that the chain is properly discretized so that a half-A and half-B segment shown in Fig. 3(b) is present at the position f, and $u-t$ is always an integer multiple of Δs. The half contributions coming from both ends are represented by the primed summation. The meaning and effect of the half-A and half-B segment will be discussed later.

For the time being, let us use the bead-spring (BS) model, which is a very common choice in polymer physics. In the BS model, neighboring segments are connected by one spring bond whose length a represents the root-mean-square (rms) average of a random step. The free energy of the chain segments $[s_1, s_2]$ in an external field $w(\mathbf{r})$ is given as

$$\Delta\mathbf{r}_\alpha(s) \equiv \mathbf{r}_\alpha(s) - \mathbf{r}_\alpha(s-\Delta s), \tag{4a}$$

$$\frac{E(\mathbf{r}_\alpha; s_1, s_2)}{k_\mathrm{B}T} = \frac{1}{N} \sum_{s\in\{s_1+\Delta s,\ldots,s_2\}} \frac{3}{2a^2\,N}\left[\frac{\Delta\mathbf{r}_\alpha(s)}{\Delta s}\right]^2 + \frac{1}{N}\sum_{s\in\{s_1,\ldots,s_2\}}{}' w_\kappa(\mathbf{r}_\alpha(s)). \tag{4b}$$

The prefactor $3/2a^2N$ represents the strength of the spring, and it is properly chosen to make the rms end-to-end distance R_0 of a noninteracting chain to be $aN^{1/2}$. The field is defined in a way that one κ-type of segment (κ = A or B) at position $\mathbf{r}$ experiences $w_\kappa(\mathbf{r})/N$ of energy penalty. The subscript will be often omitted with the implicit understanding that $w(\mathbf{r})$ is properly chosen according to the s value. In the limit $N \to \infty$, this definition converges to the field in the standard SCFT, where $E[\mathbf{r}_\alpha; s_1, s_2]$ is a functional depending on the function $\mathbf{r}_\alpha(s)$. In the discrete chain SCFT, it becomes a multivariable function with $N+1$ position variables $\mathbf{r}_\alpha(s)$ ($s \in \{0, \Delta s, \ldots, 1\}$).

For the full understanding of the partition functions in this SCFT formulation, let us start from the two-point partial partition function for a chain segment of length sN starting from A end whose $s=0$ segment position is fixed at $\mathbf{r}_0$,

$$q(\mathbf{r}, \mathbf{r}_0, s) = \left(\frac{2\pi}{3N}\right)^{3/2} \prod_{u\in\{0,\ldots,s\}} \left(\frac{3}{2\pi a^2}\right)^{3/2} \int d\mathbf{r}_\alpha(u) \exp\left(-\frac{E(\mathbf{r}_\alpha; 0, s)}{k_\mathrm{B}T}\right) \times (a^2N)^3 \delta(\mathbf{r}_\alpha(0) - \mathbf{r}_0)\delta(\mathbf{r}_\alpha(s) - \mathbf{r}), \tag{5}$$

and the complementary two-point partial partition function for a chain segment of length $(1-s)N$ starting from B end whose $s=1$ segment position is fixed at $\mathbf{r}_1$,

$$q^\dagger(\mathbf{r}, \mathbf{r}_1, s) = \left(\frac{2\pi}{3N}\right)^{3/2} \prod_{u\in\{s,\ldots,1\}} \left(\frac{3}{2\pi a^2}\right)^{3/2} \int d\mathbf{r}_\alpha(u) \exp\left(-\frac{E(\mathbf{r}_\alpha; s, 1)}{k_\mathrm{B}T}\right) \times (a^2N)^3 \delta(\mathbf{r}_\alpha(s) - \mathbf{r})\delta(\mathbf{r}_\alpha(1) - \mathbf{r}_1). \tag{6}$$

In the standard SCFT, it is required to perform a path integral following all the possible paths of a polymer chain.[8,21] In the current SCFT formalism, however, the partition functions are products of many normal integrals over the space. Such a change allows us to identify the exact prefactors of the partition functions which are often ambiguously written in the functional integral version. In a formal language, the continuous limit of this product of discrete integrals corresponds to the functional integral of the standard SCFT.

After some algebraic derivation found in the supplementary material, we can obtain the recursive integral equation of the partition function as

$$g(\mathbf{r}) \equiv \left(\frac{3}{2\pi a^2}\right)^{3/2} \exp\left(-\frac{3\mathbf{r}^2}{2a^2}\right), \tag{7a}$$

$$q(\mathbf{r}, \mathbf{r}_0, s+\Delta s) = \exp\left(-\frac{w(\mathbf{r})}{2N}\right) \int d\mathbf{R}\, g(\mathbf{R}) \times \exp\left(-\frac{w(\mathbf{r}-\mathbf{R})}{2N}\right) q(\mathbf{r}-\mathbf{R}, \mathbf{r}_0, s), \tag{7b}$$

where the bond function $g(\mathbf{r})$ naturally emerges to specify the one-step distribution. It is currently a simple Gaussian function because we adopted the BS model. The complementary function $q^\dagger(\mathbf{r}, \mathbf{r}_1, s)$ satisfies essentially the same equation except that $s+\Delta s$ on the left-hand side is replaced by $s-\Delta s$.

The two-point partial partition functions are rarely used in the actual SCFT calculation,[46] and it is customary to use the following one-point partial partition functions:

$$q(\mathbf{r}, s) \equiv \frac{1}{(a^2N)^{3/2}} \int d\mathbf{r}_0\, q(\mathbf{r}, \mathbf{r}_0, s), \tag{8a}$$

$$q^\dagger(\mathbf{r}, s) \equiv \frac{1}{(a^2N)^{3/2}} \int d\mathbf{r}_1\, q^\dagger(\mathbf{r}, \mathbf{r}_1, s), \tag{8b}$$

with the naturally determined initial conditions $q(\mathbf{r}, 0) = q^{\dagger}(\mathbf{r}, 1) = 1$. One can directly confirm that these functions satisfy the same evolution equation as the two-point partial partition functions. Here is a summary of the process of calculating the unknown $q(\mathbf{r}, s + \Delta s)$ from the known $q(\mathbf{r}, s)$,

$$q^{*}(\mathbf{r}) = \exp\left(-\frac{w(\mathbf{r})}{2N}\right) q(\mathbf{r}, s), \tag{9a}$$

$$q^{**}(\mathbf{r}) = \int d\mathbf{R}\, g(\mathbf{R}) q^{*}(\mathbf{r} - \mathbf{R}), \tag{9b}$$

$$q(\mathbf{r}, s + \Delta s) = \exp\left(-\frac{w(\mathbf{r})}{2N}\right) q^{**}(\mathbf{r}). \tag{9c}$$

The evolution of $q^{\dagger}(\mathbf{r}, s)$ follows the same equations except that now s is decreasing.

Equation (9) looks slightly different from the familiar form found in the discrete chain SCFT literature,[21,30,41,43,45] but it produces the same results because the physical description is the same as explained below. As we have followed, the formal derivation of the integral equation (9) requires some algebra, but once it is established, its physical meaning is not so difficult to understand. Let us assume that the sNth segment is shown at the left end of the chain in Fig. 4(a) marked by the first purple line, and its unnormalized probability is given by the partition function $q(\mathbf{r}, s)$. One half-segment is positioned at $\mathbf{r}$, and the exponential function in Eq. (9a) is the proper Boltzmann factor accounting for the probability increase or decrease due to the half-segment. Then, the propagation of one random step is calculated by the integral of Eq. (9b), where the step distribution is given by the function $g(\mathbf{r})$. Now, we are at the $(s + \Delta s)N$th segment marked by the second purple line in Fig. 4(a), and $\mathbf{r}$ represents its current position. The Boltzmann factor for the new half-segment is multiplied in Eq. (9c). In this way, the three equations calculate the partial partition function evolution from the midpoint of sNth segment to the midpoint of $(s + \Delta s)N$th segment.

In this process, by using $w_{\mathrm{A}}(\mathbf{r})$ in both Eqs. (9a) and (9c), we are applying the "A evolution" shown in Fig. 4(b). After s crosses f, we must use $w_{\mathrm{B}}(\mathbf{r})$ in both Eqs. (9a) and (9c) which makes the "B evolution" shown in Fig. 4(c). Later, when we adopt the $N - 1$ bond model, we do not use a half-A and half-B segment in the modeling process. In this case, one bond inevitably connects an A segment to a B segment, and a special building block shown in Fig. 4(d) becomes necessary. For this step, $w_{\mathrm{A}}(\mathbf{r})$ and $w_{\mathrm{B}}(\mathbf{r})$ must be used alternatively in Eqs. (9a) and (9c), depending on the s evolution direction.

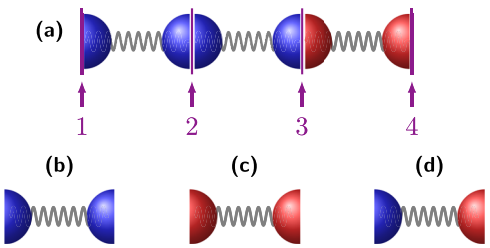

FIG. 4. (a) Schematic description of the partition function calculation for the positions 1 → 2 → 3 → 4. At position 3, $s = f$ and the segment type switches from A(blue) to B(red). Description of (b) A evolution and (c) B evolution required for the process of (a). (d) A possible alternative choice, half-A and half-B evolution.

In previous SCFT research studies using the discrete chain model,[30,41,43,45] they calculate the evolution of the partial partition function from one full-segment to the next full-segment by accounting Boltzmann weight for the field acting on a full-segment, and this causes the shape difference of the recursive integral. In our algebraic formulation, the use of half-segments makes the implementation of both real space and pseudospectral methods simpler and the resulting equations are similar to the standard SCFT as shown below.

One of the primary advantages of the discrete chain SCFT is that after the derivation of the three-step integral equations, various types of bonds can be implemented without repeating all the algebraic derivations. As long as each step is independent of the previous step, the entire properties of the bond are contained in the shape of $g(\mathbf{r})$, and it is all we need to vary. For example, if we want to use the freely jointed bond instead of the spring bond, the proper bond function is

$$g(\mathbf{r}) = \frac{\delta(|\mathbf{r}| - a)}{4\pi a^2}. \tag{10}$$

After the calculation of the partial partition functions, we can calculate the densities of A and B type segments, which are defined by the formal ensemble average of Eq. (3). Fortunately, we do not need to perform the complicated multivariable integrals for the ensemble average because the following simple summations and integral provide efficient density calculation. The A and B segment densities in the system are

$$\phi_{\mathrm{A}}(\mathbf{r}) = \sum_{\alpha} \left\langle \hat{\phi}_{\alpha,A}(\mathbf{r}) \right\rangle = \frac{V}{NQ} \sum_{s \in \{0,\ldots,f\}}{}' q(\mathbf{r}, s) q^{\dagger}(\mathbf{r}, s), \tag{11a}$$

$$\phi_{\mathrm{B}}(\mathbf{r}) = \sum_{\alpha} \left\langle \hat{\phi}_{\alpha,B}(\mathbf{r}) \right\rangle = \frac{V}{NQ} \sum_{s \in \{f,\ldots,1\}}{}' q(\mathbf{r}, s) q^{\dagger}(\mathbf{r}, s), \tag{11b}$$

where $V = n_p N \rho_0^{-1}$ is the system volume, and the total partition function Q is evaluated from the partial partition functions as follows:

$$Q[w] = \int d\mathbf{r}\, q(\mathbf{r}, s) q^{\dagger}(\mathbf{r}, s). \tag{12}$$

For more detailed proof of Eqs. (11) and (12), see the supplementary material.

Regarding the SCFT formulation of the $N - 1$ bond model which is another major tool we are going to use here, it requires only a few modifications to the above equations. For simplicity, we assume the situation of Fig. 3(a) with N segments and $N - 1$ bonds without any color split segments by choosing an integer fN. Fortunately, switch between the models does not require any complicated modification, and the idea of Fig. 4, calculating the evolution from the midpoint of one segment to the midpoint of the next segment, can be still utilized regardless of the chain model. When the $N - 1$ bond model is used, the main difference is the initial conditions of the partial partition functions

$$q(\mathbf{r}, 0) = \exp\left(-\frac{w_{\mathrm{A}}(\mathbf{r})}{2N}\right), \tag{13a}$$

$$q^{\dagger}(\mathbf{r}, 1) = \exp\left(-\frac{w_{\mathrm{B}}(\mathbf{r})}{2N}\right). \tag{13b}$$

With these initial conditions, we can use Eq. (9) for the evolution of $q(\mathbf{r}, s)$. Note that at the moment s is crossing f, we must apply the evolution of Fig. 4(d) which requires an alternative use of $w_A(\mathbf{r})$ and $w_B(\mathbf{r})$ inside the exponential functions. After the partial partition functions are calculated, the A and B segment densities can be obtained by the following equation in which nonprimed summations are now adopted

$$\phi_A(\mathbf{r}) = \frac{V}{NQ} \sum_{s\in\{0,..,f-(1-f)\Delta s\}} q(\mathbf{r},s)q^\dagger(\mathbf{r},s), \tag{14a}$$

$$\phi_B(\mathbf{r}) = \frac{V}{NQ} \sum_{s\in\{f+f\Delta s,..,1\}} q(\mathbf{r},s)q^\dagger(\mathbf{r},s), \tag{14b}$$

where $f-(1-f)\Delta s$ indicates the point of A segment just before the junction of the chain, and the point $f+f\Delta s$ corresponds to the B segment just after the junction.

Before proceeding to the next subject, let us briefly discuss the finite length effect by comparing the N bond model and $N-1$ bond model. In the $N-1$ bond model, the chain is represented by N segments, but the number of bonds is actually $N-1$, and $R_0 = a(N-1)^{1/2}$ is now the natural end-to-end length, and thus one must be careful when normalizing the length by R_0. It is slightly shorter than the well-known expression $aN^{1/2}$, and this difference is often ignored with the justification that it is negligible in the long chain limit. However, it is not a small difference to ignore for the short and intermediate length chains we are interested in.

There exists another finite length effect which is often overlooked. One usually uses $R_g^2 = a^2N/6$ as the square of the radius of gyration, but calculation with the assumption that the mass is discretely concentrated at the segment position shows $R_g^2 = a^2N(N+1)/6(N-1)$. The required correction term is $O(1)$, and it does not vanish even in the limit $N\to\infty$. Expressing all the equations using $N' \equiv N-1$ allows us to write $R_0 = aN'^{1/2}$, but this policy does not help one to reduce the error in the radius of gyration expression.

For the N bond model, because of the presence of the two half-segments, now the number of bonds is N and the natural end-to-end distance is $R_0 = aN^{1/2}$. In addition, calculation of R_g assuming that the mass is discretely concentrated at the segment position results in a value $R_g^2 = a^2(N/6 + 1/12N)$. It is much closer to $a^2N/6$ compared to the $N-1$ bond model, and the correction term is $O(1/N)$.

Now, all the partition function related equations of the discrete chain SCFT are presented, and the remaining task is to find the self-consistently determined potential fields. The story of the field transformation and the saddle point approximation remains essentially the same as those of the standard SCFT.[8,21] We omit the details here and present only the result which is consistent with our intuition

$$w_A(\mathbf{r}) = \chi N\phi_B(\mathbf{r}) + \xi(\mathbf{r}), \tag{15a}$$

$$w_B(\mathbf{r}) = \chi N\phi_A(\mathbf{r}) + \xi(\mathbf{r}), \tag{15b}$$

where χ is the interaction parameter and $\xi(\mathbf{r})$ is the pressure field enforcing incompressibility which acts equivalently on both A and B segments.

To find the self-consistent solution to these equations, it is common to use an iterative method as summarized in Fig. 5 for the $N-1$ bond model. Starting from the input fields $w_A^{in}(\mathbf{r})$ and $w_B^{in}(\mathbf{r})$, iteration continues until the output fields essentially become the same as the input fields. After the final self-consistent mean field solution is obtained, the free energy of the system is calculated by the following equation:

$$\frac{F}{n_p k_B T} = -\ln\left(\frac{Q}{V}\right) + \frac{1}{V}\int d\mathbf{r}\Big(\chi N\phi_A(\mathbf{r})\phi_B(\mathbf{r}) - w_A(\mathbf{r})\phi_A(\mathbf{r}) - w_B(\mathbf{r})\phi_B(\mathbf{r})\Big). \tag{16}$$

The last subject of this section is the finite-range interaction between the nonbonded segments. The standard SCFT formulation assumes that a segment is pointlike and the interaction between A

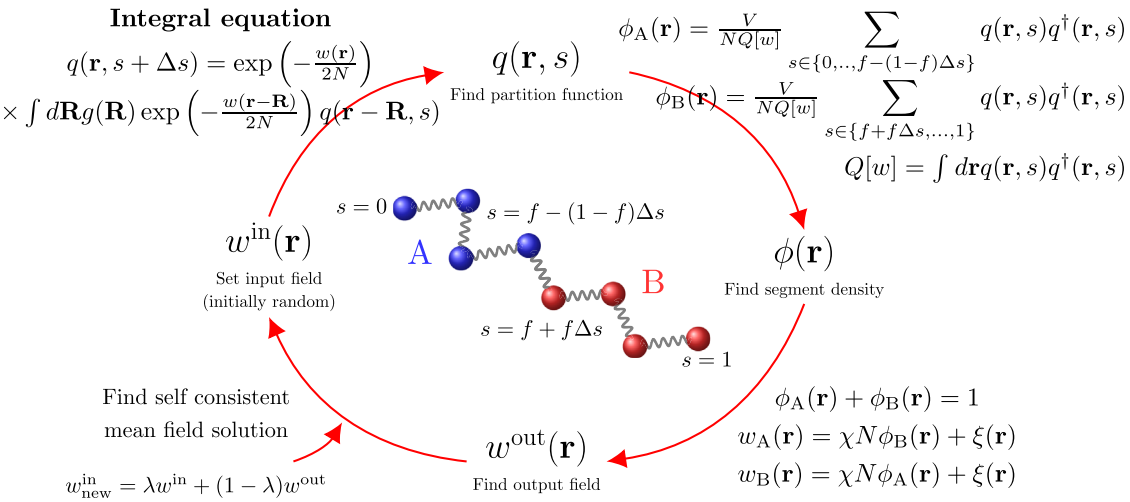

FIG. 5. Problem solving strategy of the discrete chain SCFT adopting the $N-1$ bond model.

and B type segments is counted only when they make direct contact. One advantage of the discrete chain SCFT is that it can naturally adopt an interaction potential which has a finite-range related to the bond length.[45] With this modification, the self-consistent field is determined as

$$w_A(\mathbf{r}) = \xi(\mathbf{r}) + \chi N \int d\mathbf{R}\, u(\mathbf{R})\phi_B(\mathbf{r}-\mathbf{R}), \tag{17a}$$

$$w_B(\mathbf{r}) = \xi(\mathbf{r}) + \chi N \int d\mathbf{R}\, u(\mathbf{R})\phi_A(\mathbf{r}-\mathbf{R}). \tag{17b}$$

The function $u(\mathbf{r})$ represents the strength of the interaction between A and B segments separated by $\mathbf{r}$, and it naturally emerges from the interaction energy adopting finite-ranged AB interaction[47] as follows:

$$\frac{U}{n_p k_B T} = \frac{\chi N}{V} \int d\mathbf{r} d\mathbf{r}'\, u(\mathbf{r}-\mathbf{r}')\phi_A(\mathbf{r})\phi_B(\mathbf{r}'), \tag{18a}$$

$$\int d\mathbf{r}\, u(\mathbf{r}) = 1. \tag{18b}$$

It is natural to assume that $u(\mathbf{r})$ is a simple Gaussian function which only depends on the magnitude of $\mathbf{r}$. To recover the contact interaction model, we only need to set $u(\mathbf{r}) = \delta(\mathbf{r})$. With the presence of the finite-range interaction, the free energy is now obtained by simply replacing $\phi_A(\mathbf{r})$ in the first term inside the integration of Eq. (16) by $\phi'_A(\mathbf{r}) \equiv \int d\mathbf{R}\, u(\mathbf{R})\phi_A(\mathbf{r}-\mathbf{R})$.

In principle, the field equations of the finite-range theory must be verified using the field theoretical transformation and saddle point approximation. The process is practically identical to the standard SCFT,[8] and the intuitive mean field equation (17) with a convolution form naturally results from the functional derivative of the free energy including the finite-range interaction Eq. (18).

IV. PSEUDOSPECTRAL METHOD

In this section, we will briefly introduce the pseudospectral method which is commonly used in the research using the standard SCFT. Then, we will discuss applicability of the pseudospectral method for the discrete chain SCFT calculation. More detailed issues concerning its numerical implementation follow in Sec. V.

In the standard SCFT, the solutions of most polymer problems are obtained by applying some numerical approximations to the modified diffusion Eq. (1). The numerical methods developed so far can be categorized into three groups: (i) real space method,[22,23,48–57] (ii) spectral method,[8,24] and (iii) pseudospectral method.[56–63] Nowadays, real space and pseudospectral methods are mainly used to find the nanoscale morphology of a given polymeric system.

To obtain a numerical solution using the real space method, it is common to divide the system volume with M_1, M_2, and M_3 grids in each direction, and the Laplacian is approximated by the finite difference method (FDM) or finite volume method (FVM) incorporated with the Crank-Nicolson method[57,64] or its approximation, alternating direction implicit (ADI) method.[54,56,57,64] We will not explain the details of the real space method, but it is necessary to mention the speed of the numerical algorithm. In the real space method, the unknown function $q(\mathbf{r}, s+\Delta s)$ is calculated from the known function $q(\mathbf{r}, s)$, where Δs is the discretized step size in the s direction. The Crank-Nicolson method is known to be slow, but when the ADI method is adopted, a fast calculation is possible with $O(M)$ time where $M = M_1M_2M_3$ is the spatial grid number.

In the pseudospectral method of the standard SCFT, the spatial discretization is essentially the same as the above description. The one-step advance of the partial partition function $q(\mathbf{r}, s)$ in the s direction is now calculated by the following three-step operator splitting method:[57–59]

$$q^*(\mathbf{r}) = \exp\left(-\frac{\Delta s}{2} w(\mathbf{r})\right) q(\mathbf{r}, s), \tag{19a}$$

$$q^{**}(\mathbf{r}) = \exp\left(-\frac{\Delta s}{6} \nabla^2\right) q^*(\mathbf{r}), \tag{19b}$$

$$q(\mathbf{r}, s+\Delta s) = \exp\left(-\frac{\Delta s}{2} w(\mathbf{r})\right) q^{**}(\mathbf{r}). \tag{19c}$$

Note that it is implicitly assumed that $w(\mathbf{r})$ is properly chosen according to the s value. The nontrivial step is Eq. (19b) where a rescaled Laplacian operator appears in the exponential function.

Instead of calculating this in the real space, the pseudospectral method performs Fourier and inverse Fourier transforms before and after this step, respectively. As a consequence, the differentiation in the real space is converted to a simple multiplication in the Fourier space. For the pseudospectral method, the most time-consuming operation is the Fourier and inverse Fourier transforms, and the required time for the one-step advance in the s direction is $O(M \log M)$ when fast Fourier transform (FFT) is used. With the help of modern FFT packages such as fastest Fourier transform in the west (FFTW),[65] the actual calculation speed of the pseudospectral method can be as fast as that of the real space calculation adopting the ADI method.

Before examining the applicability of the pseudospectral method in the discrete chain SCFT, it is the proper time to discuss the speed of real space calculation of the recursive integral equation (9b). The shape of the integral implies that one three-dimensional integral is necessary for every point $\mathbf{r}$, and the one-step evolution requires $O(M^2)$ operations where M is the spatial grid number; thus, the real space calculation of discrete chain SCFT is inevitably slower than the standard SCFT whose time complexity can reduce to $O(M)$ or $O(M \log M)$ with the adoption of the fastest algorithms. If we apply an appropriate cutoff to the bond function $g(\mathbf{r})$, the performance can be greatly enhanced because we now use only a small part of the total volume for each $\mathbf{R}$ integral. Nevertheless, the real space calculation of discrete chain SCFT cannot compete with the standard SCFT in terms of speed, and it is not a practical tool for the simulation of three-dimensional polymeric systems.

One suggestion to overcome this problem is the use of the pseudospectral method as verified in the standard SCFT research. Even though it is natural to conceive the adoption of the pseudospectral method for the evaluation of the recursive equations,[21,45] the practicality of the algorithm has not been verified in that no known research has implemented this technique for the study of real polymer systems. The idea of the pseudospectral calculation of the integral seems to be straightforward, but we have found some troublesome issues in the implementation of the pseudospectral method, and the details will be discussed in Sec. V.

Our formulation developed so far is carefully designed for the future adoption of the numerical algorithms; the evolution of the partition function calculated by the three steps displayed in Eq. (9)

has a very similar structure to that of the pseudospectral or the operator splitting real space methods[57,66] of the standard SCFT. The most time-consuming step of the real space calculation is the integral of Eq. (9b), and because it has the shape of a convolution integral, one natural suggestion is to perform this calculation in the Fourier space where the convolution integral becomes a simple multiplication

$$\tilde{q}^{**}(\boldsymbol{\xi}) = \tilde{g}(\boldsymbol{\xi})\tilde{q}^{*}(\boldsymbol{\xi}). \tag{20}$$

In this paper, we use the notation that the tilde on a variable denotes its Fourier transform or Fourier cosine transform. The Fourier transform is defined in the following way:

$$\tilde{f}(\boldsymbol{\xi}) \equiv \int d\mathbf{r}\, f(\mathbf{r}) \exp(-2\pi i \boldsymbol{\xi}\cdot\mathbf{r}). \tag{21}$$

For the BS model, the Fourier transform of the Gaussian distribution function is another Gaussian in the $\boldsymbol{\xi}$ space

$$\tilde{g}(\boldsymbol{\xi}) = \exp\left(-\frac{2}{3}\pi^2 a^2 |\boldsymbol{\xi}|^2\right). \tag{22}$$

In its numerical implementation using M spatial grids, we use the discrete Fourier transform (DFT) which can be performed by $O(M \log M)$ operations, and this is essentially the time complexity of the single evolution step. Considering that the Fourier and inverse Fourier transforms are performed just before and after Eq. (9b), researchers accustomed to the standard SCFT would recall the pseudospectral method of it. Indeed, with a special combination of the N bond model and BS model, the discrete chain SCFT calculation becomes equivalent to the calculation of the standard SCFT using the standard pseudospectral method with $\Delta s = 1/N$.

V. NUMERICAL IMPLEMENTATION

A. Bond function discretization

Since space must be discretized in the numerical calculation, all the real space functions are represented by a set of discrete points. In this approach, Fourier transform must be replaced by its discrete version, DFT. However, this conversion is not a trivial task because naïve discretization of the bond function $g(\mathbf{r})$ is prone to amplify errors in the calculation of the partition function, and material conservation is known to be an important issue.[57]

With this in our mind, let us start implementing the numerical scheme using a simple three-dimensional box of size L_x, L_y, and L_z, and each direction is discretized by Δx, Δy, and Δz so that an integer vector $\mathbf{i} = (i, j, k)$ represents the grid point on the position $\mathbf{r_i} \equiv (i\Delta x, j\Delta y, k\Delta z)$. The discretized partition function value at each point is $q_\mathbf{i} \equiv q_{i,j,k}$ where each index starts from 0, and the maximum values of i, j, and k are $I \equiv L_x/\Delta x$, $J \equiv L_y/\Delta y$, and $K \equiv L_z/\Delta z$, respectively, when the periodic or Neumann boundary conditions are applied in all directions.

The spatial integral is now evaluated by a weighted summation

$$\int d\mathbf{r}\, f(\mathbf{r}) \to \sum_{\mathbf{r_i}} f(\mathbf{r_i})\Delta V_\mathbf{i}, \tag{23}$$

where $\Delta V_\mathbf{i}$ is the volume of the $\mathbf{i}$th cell. For equally spaced Cartesian grids, most of $\Delta V_\mathbf{i}$ are $\Delta V \equiv \Delta x \Delta y \Delta z$, but factors 1/2, 1/4, and 1/8 are multiplied when the point (i, j, k) is at the planar, line, and vertex boundaries, respectively.

Let us make a careful thought about the discretization of the bond function $g(\mathbf{r})$ using the one-dimensional BS model as an example. For the one-dimensional problem, we will always consider a system with z dependent functions, assuming symmetry in x and y directions. Now the required job is to discretize the Gaussian distribution function $g(z) = (3/2\pi a^2)^{1/2} \exp(-3z^2/2a^2)$. Because the space is discretized by Δz, one is tempted to directly use $g_k \equiv g(k\Delta z)$ as the discrete distribution function and try to perform DFT of them. With this choice, however, the weighted summation $\sum g_k \Delta V_k$ is not exactly equal to 1, which means that the total probability of one step is not equal to 1. Another issue is the tail of the distribution function. In principle, $g(z)$ is defined at $z \in (-\infty, \infty)$, but we need to set $g(z) = 0$ for large enough $|z|$ to provide appropriate cutoffs for the integral of Eq. (9b). Let us accept a very loose condition for the time being, $g(z) = 0$ for $|z| > L_z$. For the three-dimensional distribution function, x and y directional cutoffs are given accordingly.

Here is a simple solution to both issues, regardless of the dimensionality of the system. In the previous report of Yong and Kim,[57] it was shown that the probability or material conservation and the constant rms step size are two important rules one must keep in the numerical SCFT calculation. Such a consideration suggests us to adopt a discrete distribution function $g_\mathbf{i}$ satisfying the following two equations:

$$\sum g_\mathbf{i} \Delta V_\mathbf{i} = 1, \tag{24a}$$

$$\sum \mathbf{r}_\mathbf{i}^2 g_\mathbf{i} \Delta V_\mathbf{i} = a^2. \tag{24b}$$

The first equation guarantees the probability conservation, while the second equation is for the fixation of the rms step size in the discrete calculation. It is a relatively easy task to slightly modify the height and width of the Gaussian function of the BS model to satisfy these two equations, and our test shows that such a slight deviation does not create any noticeably undesirable side effect. Thus, we always use Eq. (24) regardless of the choice of the bond model and the distribution function. After obtaining the discretized values of the modified distribution function in real space, DFT is applied, and simple multiplication of Eq. (20) is performed in the Fourier space without violating the mass conservation condition.

The implementation of the FJC model is a more challenging task because of the delta function shaped $g(\mathbf{r})$. At least its one-dimensional version is easier to construct to satisfy Eq. (24) because the bond function $g(z)$ reduces to a step function[30]

$$g(z) = \begin{cases} 1/2a, & \text{if } |z| \le a, \\ 0, & \text{otherwise.} \end{cases} \tag{25}$$

Because of its finite range, this model is easier to implement compared to the one-dimensional BS model, and relatively faster calculation of Eq. (9b) is possible by making cutoffs at $z = \pm a$. We again warn that the probability conservation error may be significant if a naïve discretization of the step function, $g_k \equiv g(k\Delta z)$, is chosen. As suggested earlier for the Gaussian function, by making a slight modification to the step height and width, Eq. (24) can be easily matched, and this is the recommendable way to implement the pseudospectral method in the discrete chain SCFT.

The true challenge is the full three-dimensional calculation of the FJC model. In this case, the Dirac delta function in $g(\mathbf{r})$ makes the spatial discretization in real space rather difficult. We do not

recommend its direct implementation in real space, and this issue will be discussed in Subsection V B.

B. Three-dimensional FJC model

In Subsection V A, the implementation of the Dirac delta function shaped $g(\mathbf{r})$ was a difficult task for the three-dimensional spatial grid. At practically no grid point $(i\Delta x, j\Delta y, k\Delta z)$, the function value is nonzero, but it is required to assign some values on the grids to represent the delta function while satisfying Eq. (24), and do not forget that we also need its Fourier transform for the pseudospectral calculation. Fortunately, at least part of these issues disappear if we start the discretization in the discrete Fourier space because the three-dimensional Fourier transform of the FJC bond function is analytically calculated as[21,45]

$$\tilde{g}(\boldsymbol{\xi}) = \mathrm{sinc}(2|\boldsymbol{\xi}|a) \equiv \frac{\sin(2\pi|\boldsymbol{\xi}|a)}{2\pi|\boldsymbol{\xi}|a}. \tag{26}$$

This is a smooth function in the Fourier space, and it can be easily discretized in the discrete Fourier space.

For example, when the Neumann boundary condition is used, discrete cosine transform (DCT) is naturally adopted, and $\tilde{g}_{\mathbf{i}}$ can be taken by sampling of $\tilde{g}(i/2L_x, j/2L_y, k/2L_z)$, which becomes

$$\tilde{g}_{\mathbf{i}} = \frac{1}{8\Delta V}\,\mathrm{sinc}\left(a\sqrt{\left(\frac{i}{L_x}\right)^2 + \left(\frac{j}{L_y}\right)^2 + \left(\frac{k}{L_z}\right)^2}\right), \tag{27}$$

where the range of each index is from 0 to its maximum value, I, J, or K. When the boundary conditions are periodic, DFT is now adopted, and the $\tilde{g}_{\mathbf{i}}$ can be obtained by sampling of $\tilde{g}(i/L_x, j/L_y, k/L_z)$, with the additional consideration on its periodic property. Thus,

$$\tilde{g}_{\mathbf{i}} = \frac{1}{\Delta V}\,\mathrm{sinc}\left(2a\sqrt{\left(\frac{i'}{L_x}\right)^2 + \left(\frac{j'}{L_y}\right)^2 + \left(\frac{k'}{L_z}\right)^2}\right), \tag{28}$$

where $i' = i$ if $i < I/2$ and $i' = i - I$ otherwise. j' and k' are defined similarly. In this paper, we show our calculations using DCT adopting Neumann boundary conditions.

When the entire calculations are performed in the Fourier space, it is an attractive idea to use this $\tilde{g}_{\mathbf{i}}$ function. For example, in a low molecular weight diblock copolymer research using the spectral method, Matsen has used the sinc function for the evaluation of the convolution integral in the Fourier space for the purpose of obtaining the phase diagram.[45]

However, the real space function obtained by performing inverse DCT of Eq. (27) is somewhat unsatisfactory in terms of the reproducibility of the original function and non-negativity of the probability. Figures 6(a) and 6(b) exhibit the reconstructed delta function distribution of Eq. (10) on the two planes, $z = 0$ and $z = 4a/5$, for the case of $\Delta x = \Delta y = \Delta z = a/10$. As expected, Fig. 6(a) shows that $g_{\mathbf{i}}$ is highly peaked at the grid cells where the circle $x^2 + y^2 = a^2$ passes. The nontrivial feature is that the probability is also distributed to the cells which do not contain the circle. What makes things worse is that cells far from the circle exhibit finite amplitudes and sometimes $g_{\mathbf{i}}$ even becomes slightly negative. The amplitude plot for the plane $z = 4a/5$ [Fig. 6(b)] shows a similar

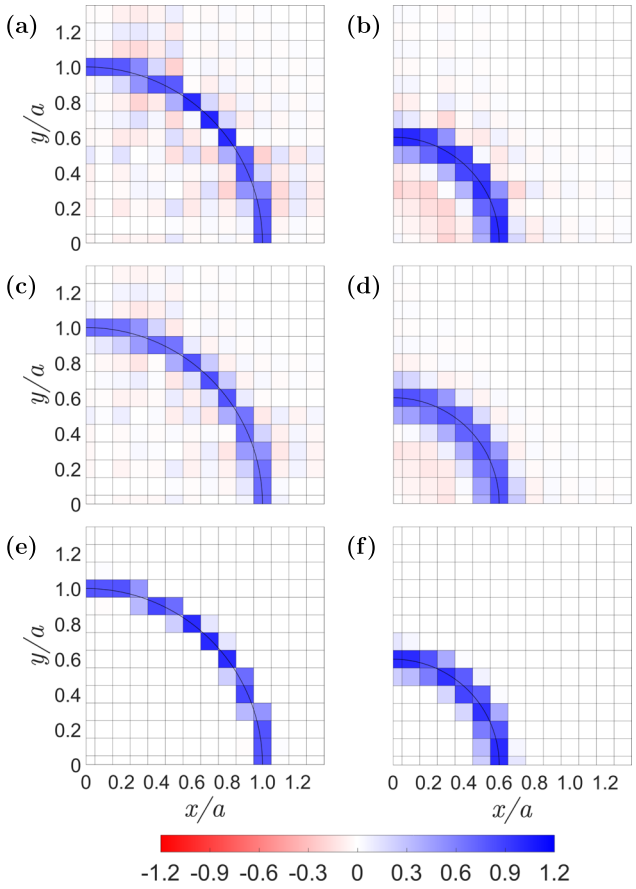

FIG. 6. (a) $g_{i,j,0}$ and (b) $g_{i,j,8}$ of the FJC model obtained by Eq. (27) for the case of $\Delta x = \Delta y = \Delta z = a/10$. (c) $g_{i,j,0}$ and (d) $g_{i,j,8}$ obtained by Eq. (30) after using only $n_x = n_y = n_z = 0$. (e) and (f) are the results with the summation up to $n_x = n_y = n_z = \pm 5$.

behavior except that now $x^2 + y^2 = (3a/5)^2$ is the circle of peak amplitudes. One may worry that the negative $g_{\mathbf{i}}$ or negative probability may cause a catastrophe when using the FJC model, but the aforementioned research suggests that this local probability anomaly does not cause a serious problem.[45] Our analysis also confirms that the strong peak averages out all the negative variables in the long run, and the final segment density always becomes positive for reasonable choices of parameters.

We may instead suggest an alternative method which is based on an intuitive idea. It is obvious that $g(i\Delta x, j\Delta y, k\Delta z)$ cannot be a good candidate of $g_{\mathbf{i}}$ for the FJC model, but the average of $g(\mathbf{r})$ within the cell can be a valid candidate

$$g_{\mathbf{i}} \equiv \frac{1}{\Delta V}\int_{-\Delta z/2}^{\Delta z/2}\int_{-\Delta y/2}^{\Delta y/2}\int_{-\Delta x/2}^{\Delta x/2} \times g\left(i\Delta x - x', j\Delta y - y', k\Delta z - z'\right)dx'dy'dz'. \tag{29}$$

Applying this idea to Eq. (10), $g_{\mathbf{i}}$ of Eq. (29) now becomes the surface area of a sphere of radius a contained within the $\mathbf{i}$th cell divided by $4\pi a^2$. Even though this definition is conceptually clear, the actual calculation of the integral is not a trivial task.

Fortunately, the sampling theory of the discrete time Fourier transform (DTFT) provides an efficient method to calculate the DCT of Eq. (29) (see the Appendix for the detail). Using this method, $\tilde{g}_{\mathbf{i}}$ of the FJC bond function becomes

$$\tilde{g}_{\mathbf{i}} = \frac{1}{8\Delta V}\sum_{n_x,n_y,n_z}\operatorname{sinc}\left(a\sqrt{\left(\frac{i-2n_xI}{L_x}\right)^2+\left(\frac{j-2n_yJ}{L_y}\right)^2+\left(\frac{k-2n_zK}{L_z}\right)^2}\right) \times \operatorname{sinc}\left(\frac{i-2n_xI}{2I}\right)\operatorname{sinc}\left(\frac{j-2n_yJ}{2J}\right)\operatorname{sinc}\left(\frac{k-2n_zK}{2K}\right), \tag{30}$$

where each of the n_x, n_y, and n_z summation range is from $-\infty$ to ∞, and the inverse DCT of this expression provides us a valid $g_{\mathbf{i}}$. The convergence of this summation is surprisingly good. Figures 6(c) and 6(d) exhibit $g_{\mathbf{i}}$ obtained only by using $n_x = n_y = n_z = 0$ term, and they already look better than Figs. 6(a) and 6(b). The results with the summation up to $n_x = n_y = n_z = \pm 5$ are shown in Figs. 6(e) and 6(f). Cells with negative $g_{\mathbf{i}}$ practically disappear, and the results are almost the same as the spherical surface fraction within the cell. One last note is that the transformed $g_{\mathbf{i}}$ in the real space does not exactly satisfy Eq. (24), and thus slight adjustments are recommended for its practical implementation. The easy way is to make a small modification to the function $\tilde{g}_{\mathbf{i}}$ in Eq. (30) to satisfy Eq. (24).

Discretization of a quickly varying function results in a significant loss of high frequency modes. Averaging within the cell using Eq. (29) can be viewed as a filtering process eliminating high frequency mode of bond function, and it is the reason why our approach has been successful for the FJC bond function. This filtering approach can be easily applied to other bond functions whose analytic Fourier transforms are known, and we expect that a better spatial discretization is achievable especially when the bond function is a quickly varying function. All we need to do is to replace the first sinc function of Eq. (30) with the known Fourier transform of the bond function while leaving the last three sinc functions.

In the development stage of discrete chain SCFT, the real space method[30] was naturally used, and the full spectral method[45] was adopted later for the purpose of creating the block copolymer phase diagram. Slow speed was not a crucial issue in the development stage, but for a new theoretical framework to be widely accepted, it is important to show that a fast calculation is possible, and the pseudospectral method provides the perfect solution.

We perform a speed test of the three-dimensional discrete chain SCFT pseudospectral method using a single core of Xeon Gold 6132 CPU, and the DCTs are performed with the FFTW package.[65] For the test system, we take the diblock copolymers with parameters $N = 50$, $\chi N = 25$, and $f = 0.2$, which is expected to create a body-centered-cubic phase. When the FJC bond function and $32 \times 32 \times 32$ grid box are used, it takes 0.2 s per 1 iteration, and 11 s is enough to obtain the final morphology. For a larger system with a $256 \times 256 \times 256$ grid box, it takes 112 s per 1 iteration, and 93 min is required for the whole calculation. In short, the pseudospectral method of discrete chain SCFT is as fast as any known real space or pseudospectral method implementations of the standard SCFT.

C. Boundary condition issues

For the actual implementation of the pseudospectral method in the discretized world, certain boundary conditions must be chosen, and there are a few subtle physical and numerical issues that must be cleared for their proper implementation. When the boundary condition of the $q_{\mathbf{i}}$ family is periodic with period L_x, L_y, and L_z in each direction, to apply the convolution theorem, we assume the discrete bond function $g_{\mathbf{i}}$ has the same periodicity even though $g(\mathbf{r})$ is, in principle, a nonperiodic function. One can easily check that such a modification does not do any harm for the integral of Eq. (9b), as long as one period of convolution integral is performed in all directions. To make $g_{\mathbf{i}}$ periodic and for the accuracy of the calculation, it must slightly deviate from $g(i\Delta x, j\Delta y, k\Delta z)$ while satisfying Eq. (24).

The case with the Neumann boundary is somewhat more complicated. Under the condition that $g(\mathbf{r})$ has the reflection symmetry with respect to $x = 0$, $y = 0$, and $z = 0$ planes, which is usually true, the discrete version of Eq. (20), $\tilde{q}^{**}_{\mathbf{i}} = \tilde{g}_{\mathbf{i}}\tilde{q}^{*}_{\mathbf{i}}$, is valid with the interpretation that the tilde on a variable now represents its DCT. In other words, all we need to do is to define $g_{\mathbf{i}}$ in the region $0 \le i \le I$, $0 \le j \le J$, and $0 \le k \le K$ and perform its DCT.

One can easily imagine another common situation, the Dirichlet boundary condition, and it is sometimes adopted in the standard SCFT calculation for the modeling of the polymer-air or polymer-substrate interface. However, it is not a trivial task to model these boundaries in the discrete chain SCFT calculation. When using a Dirichlet boundary condition in solving a differential equation, we expect that the function values are zero at the boundary. In the pseudospectral method, the natural strategy is to use a discrete sine transform (DST) for the $q(\mathbf{r})$ family. Even though such a calculation is numerically possible, it is not a recommendable strategy for the modeling of interfaces in the discrete chain SCFT as explained below.

Let us consider a situation that there exists a wall at $z = 0$ so that no polymers exist at $z < 0$. When no additional interaction is imposed, we can naturally call it a neutral wall. However, one must be careful that the presence of the wall reduces the entropy of polymer chains near the wall, which creates an effective repulsion.[29,30] In the discrete chain model, the correct way to represent the nonexistence of segments beyond the wall is to let the partition function vanish whenever a segment crosses the wall. It can be achieved by setting the function value to be zero beyond the boundary wall after each integration of Eq. (9b). Earlier research studies show that when the field acting on the polymers vanishes, the polymer density at $z = 0$ is exactly $1/N$ of the bulk density,[29,30] which means that only the $N \to \infty$ limit can be legitimately called the Dirichlet boundary case. In this way, the discrete chain SCFT opens up possibility of a new interesting boundary condition, the neutral boundary, which was not available for the standard SCFT calculation with the Gaussian chain model.

When the neutral boundary condition is chosen, performing the integral of Eq. (9b) in the real space is not a particularly complicated process. However, as explained in Sec. IV, the real space calculation in three dimension is very slow, and the pseudospectral method is the preferable choice for the discrete chain SCFT. The fact that the DST is not applicable for this problem is a slight disappointment, but the pseudospectral method is still

a valid approach because all we need to do is to perform the convolution integral after enforcing $q(\mathbf{r}) = 0$ beyond the neutral walls.

To achieve this, the system boundary can be extended beyond the wall by the practical range of the bond function $g(\mathbf{r})$, and $q(\mathbf{r})$ is set to zero in the newly added space. Now the convolution integral of the total system can be performed using DFT or DCT without a problem. After the integral is finished, the extended region is removed and the original system size is restored. Such an algorithm requires an additional computational resource for the extended space, but the whole process of the one-step evolution is guaranteed to be finished in $O(M \log M)$ time, and this is certainly the best strategy of discrete chain SCFT for the two- or three-dimensional system when the neutral boundary condition is chosen. In Subsection VI B, we will use this method for the analysis of the block copolymer thin film system.

VI. COMPUTATIONAL RESULTS

A. Discrete chain behavior in lamellar morphology

As described earlier, we have a few valid modeling methods for the discrete polymer chain. In addition to the $N - 1$ bond model which is the typical choice, the N bond model is also available, and use of the BS or FJC bond function is another choice which can be combined with the previous one. Regardless of the model, the result of discrete chain SCFT must converge to the solution of the standard SCFT using the Gaussian chain model in the limit $N \to \infty$, and it allows us to use the discrete chain SCFT as an approximation of the standard SCFT. In this subsection, we make a few tests of the discrete chain SCFT using lamellar forming symmetric ($f = 0.5$) diblock copolymers adopting various chain models, and we compare the results with those of the standard SCFT. Note that $R_0 \equiv a(N-1)^{1/2}$ for the $N - 1$ bond model, and $R_0 \equiv aN^{1/2}$ is used for the N bond model.

In our experience with the standard SCFT, fine discretization in the s direction is important at high χN. Similar behavior is found in the current simulation. Figure 7 displays the block copolymer period D and the interfacial width w_I for various chain models[8] at $\chi N = 50$ and 100. For the calculation in this subsection, we use 2000 grid points for the simulation box. The spatial discretization Δz varies according to the box size, and it ranges from $0.0004R_0$ to $0.0008R_0$. Thus, for all the parameters we have utilized here, there exist enough grid numbers to accurately analyze the behavior of the interfacial width. As expected, all curves converge to the standard SCFT results in the limit $N \to \infty$, but deviations are not negligible at intermediate N values and there are a few noticeable differences between the models. For the FJC model at $\chi N = 50$, $N = 50$ is enough for D and w_I to reach to the standard SCFT results, but the BS model seems to converge slower so that somewhat higher N is required to see the convergence.

The cases with $\chi N = 100$ exhibit similar trends. For the FJC and SB models, $N = 100$ and 400 are required to confirm the convergence, respectively. Comparing between the segment models, the N bond model shows a slightly better convergence compared to the $N - 1$ bond model, which has the mismatch of the bond number $(N - 1)$ and the segment number (N). The observation that the convergence is faster for the FJC model might be a surprise for those who think that the springlike bond of the BS model makes it closer to the Gaussian chain model.

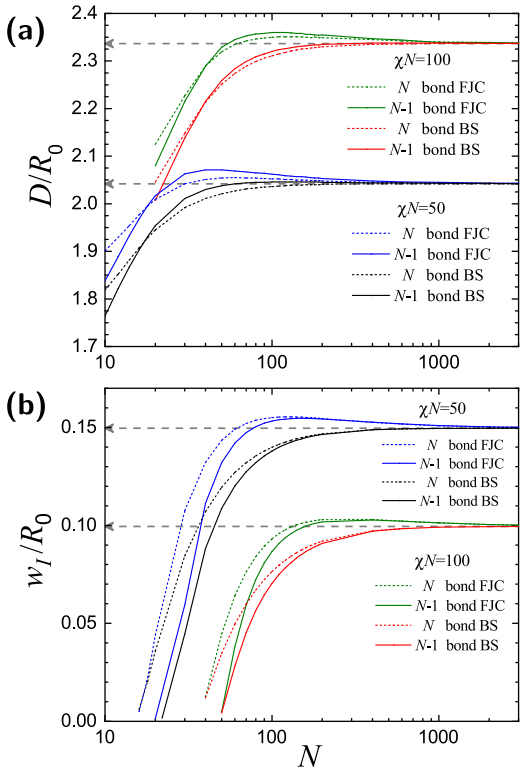

FIG. 7. (a) Lamellar period D and (b) interfacial width w_I for the discrete chain SCFT of symmetric ($f = 0.5$) AB block copolymers with $\chi N = 50$ and 100, as functions of N. The dashed lines are the standard SCFT results using the Gaussian chain model.

This issue can be investigated further by analyzing Fig. 8 which extends Matsen's analysis on the $N - 1$ bond FJC model[45] to the other possible models. In this figure, D and w_I for the various chain models are plotted as functions of χN at fixed N. For the lamellar period of the $N = 160$ case, the $N - 1$ bond model and N bond model are nearly indistinguishable for both BS and FJC models. The case with $N = 160$ shows that the lamellar period of the FJC models follows the standard SCFT result (dashed line) for χN up to 300, while that of the BS models deviates slightly from the standard SCFT result at such a large χN.

The interfacial width shown in Fig. 8(b) provides an important hint to understand this behavior. Due to the finite bond size and strong stretching near the AB interface, the A and B segments are essentially segregated at very large χN, and they form a sharp interface. Near this one-dimensional interface, one step of the bond has the Gaussian function shape in the BS model. On the other hand, the step has the shape of Eq. (25) in the FJC model, and there is a higher chance for an A segment near the interface to send its random-walking A neighbor beyond the interface and increase the degree of mixing. This residual mixing effect makes the FJC model behave more like the standard SCFT in which infinitely flexible chains easily mix. Because the lamellar period increases at increasing χN to

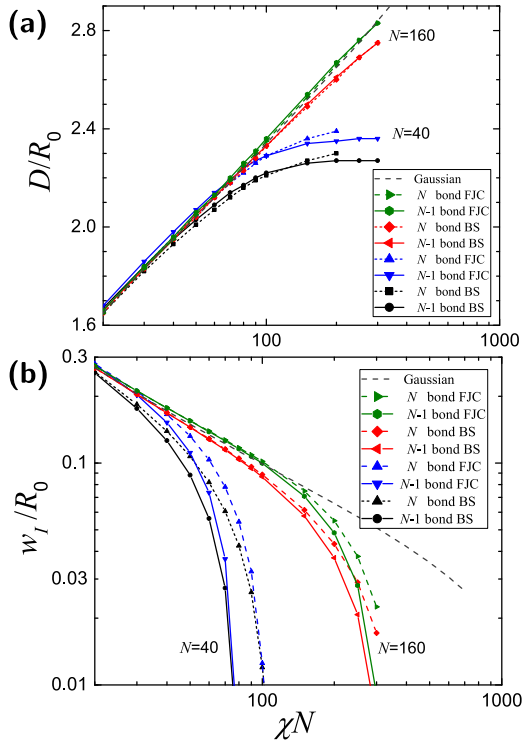

FIG. 8. Discrete chain SCFT (a) lamellar period D and (b) interfacial width w_I as functions of χN. The dashed lines are the standard SCFT results using the Gaussian chain model.

achieve better segregation between A and B blocks, the decrease in the interfacial width works in the direction to shrink the period, which can be confirmed by Fig. 8(a).

The idea that decrease in the interfacial width for highly stretched chains leads to the period reduction is consistent with the observation of Fig. 7. Surface energy plot in Sec. C of the supplementary material confirms that the interfacial energy actually decreases with decreasing N at fixed χN, and thus decrease in the interfacial width is the cause of the interfacial energy and the block copolymer period reduction.

The stronger mixing effect of the FJC model also provides an explanation to the observation of a slight overshoot of D and w_I in Fig. 7 at intermediate values of N. In this regime, due to the extra mixing of A and B segments near the interface, the interfacial width of the FJC model [Fig. 7(b)] is slightly wider than the standard SCFT case, which in turn increases the period D slightly to create the overshoot.

Figure 8 also shows that, for the shorter chains with $N = 40$, the general behaviors of the models are similar to the $N = 160$ cases except that now D and w_I deviate from the standard SCFT results at a smaller χN. At this N value, let us compare the two choices, the $N - 1$ bond and N bond models. At large enough χN, the width w_I is notably narrower for the $N - 1$ bond model. The shape of the segments displayed in Figs. 3(a) and 3(b) provides a convincing argument explaining this behavior. Because of the presence of the half-A and half-B segment, mixing of blocks is more significant in the N bond model. The lack of such a segment makes a sharper boundary and a shorter period for the $N - 1$ bond model.

B. Diblock copolymers in thin film

When lamellar forming AB block copolymers are confined in a thin film morphology, the lamellar domains may align parallel or perpendicular to the substrate. In general, when the polymer-substrate or polymer-air surface interaction is preferential to a specific block, surface-parallel lamellae are naturally chosen.[67,68] For those who wish to create surface-perpendicular lamellae, it is necessary to make a special tuning of the surface property. For example, the surface tensions of PS and poly(methyl methacrylate) (PMMA) are very similar, and PS-*b*-PMMA block copolymers are commonly used for the creation of surface-perpendicular lamellae.[69,70] The substrate must also be neutralized for the effective control of the lamellar orientation. The PS-*r*-PMMA layer,[71] self-assembled monolayer,[72] and chemically modified graphene layer[73] are often used for the neutralized substrate of PS-*b*-PMMA block copolymers.

There are a few issues concerning the theoretical treatment of the neutralized surface, especially when we consider the boundary as a hard impenetrable wall. It is well known that a polymer chain loses its conformational entropy near the wall, but the degree of entropy loss strongly depends on the bond step size and shape.[29,30,41,74,75] Because of this, the standard SCFT using infinitely flexible Gaussian chains can capture the physics near the hard wall only after adding some extra features such as a gradual density variation.[31,75–78] Another interesting approach to this problem is the lattice SCFT[32,33] which has been a branch of the SCFT family since its development stage. By introducing interaction potential which depends on the density at the nearest lattice sites, the preference of the surface-perpendicular morphology over the surface-parallel one has been successfully demonstrated using the lattice SCFT.[35,79]

In this subsection, we analyze the behavior of freely jointed block copolymers confined by the neutral walls using two-dimensional discrete chain SCFT adopting finite-range interaction. The results of the BS model are also available in section B of the supplementary material. Let us consider a symmetric ($f = 0.5$) AB block copolymers confined between two neutral walls at $z = 0$ and $z = L_z$ [see Fig. 9(a)]. For the calculation of the surface-perpendicular lamellar morphology, at least two-dimensional calculation must be used. For the following calculation, the x directional size L_x is chosen to be 1/2 times of the bulk period, and the Neumann boundary conditions are adopted in the x direction. The shape of the finite-range interaction function $u(\mathbf{r})$ is chosen as a Gaussian function

$$u(\mathbf{r}) = \left(\frac{3}{2\pi a^2}\right)^{3/2} \exp\left(-\frac{3\mathbf{r}^2}{2a^2}\right). \tag{31}$$

This choice assumes that the effective interaction range is the bond size a, which is a reasonable assumption. For the convenience of the pseudospectral method, the actual discrete function has a cut-off at $|\mathbf{r}| = 2a$, beyond which $u_\mathbf{i} = 0$, and it is normalized to satisfy Eq. (24) with $g_\mathbf{i}$ being replaced by $u_\mathbf{i}$. For the bond distribution function $g_\mathbf{i}$, two-dimensional Fourier transform of the FJC bond function is required. We adopt the DCT expression, Eq. (30), after dropping

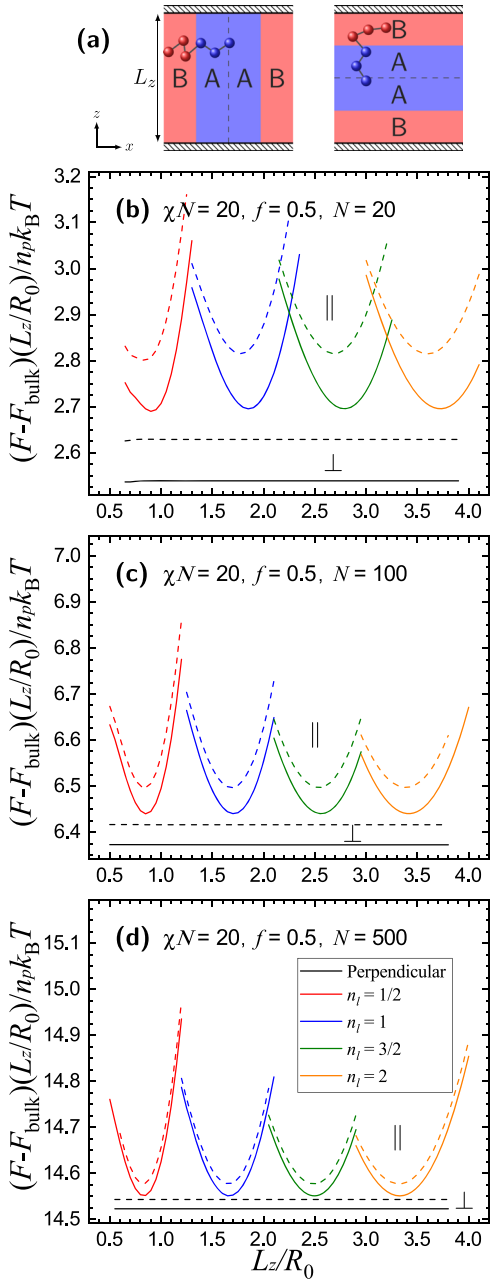

FIG. 9. (a) Schematic diagram of freely jointed AB block copolymers confined by the two neutral walls. (b) The free energy comparison between the surface-perpendicular (black lines, ⊥) and surface-parallel (colored lines, ||) morphologies with n_l periods at $\chi N = 20$, $f = 0.5$, and $N = 20$. Dashed lines are for the N bond model, and real lines are for the $N - 1$ bond model. (c) and (d) are the free energy comparison plot at $N = 100$ and $N = 500$, respectively.

the terms for the y direction, and n_x and n_z summation is made from −5 to 5. Afterward, a slight modification is made to the normalization factor for the inverse DCT of this expression to satisfy Eq. (24).

As suggested in Subsection V C, we extend the system boundary beyond the neutral wall by $2a$ in both $+z$ and $-z$ directions, and the pseudospectral method with DCT is used for the partition function calculation through the convolution integral. With this method, we manage to keep the time complexity of the one-step evolution to be $O(M \log M)$. For the field calculation, it is also required to perform a convolution integral given by Eq. (17), and the aforementioned boundary extension technique is also applicable to this calculation.

Figure 9(b) exhibits the excess free energy comparison between the surface-perpendicular and surface-parallel lamellar morphologies at $N = 20$ by using the $N - 1$ bond (solid lines) and N bond (dashed lines) FJC models. The excess free energy per chain is normalized by the dimensionless film thickness $L_z/aN^{1/2}$ so that we are essentially comparing the effective interfacial energy.[8,80] With the adoption of the finite-range interaction, the vertical lamellar morphology can reduce the energy penalty of the A-B interaction near the polymer-air or polymer-substrate interface, and thus a clear energy gap exists even when L_z is an integer multiple of $L_0/2$ which is the commensurate film thickness. The gap turns out to be independent of the layer number n_l, which is consistent with the idea that this gap corresponds to the surface tension difference of the two morphologies.

The free energy behaviors of the two morphologies at $N = 100$ and $N = 500$ are also plotted in Figs. 9(c) and 9(d), respectively. One can observe a clear reduction of the free energy gap as N increases. It is because the difference between the discrete chain SCFT and standard SCFT reduces as N increases, and they become identical at $N \to \infty$. In this limit, our interaction model with range a reduces to the contact interaction model, and thus we recover the result of the standard SCFT in which the free energy gap is known to vanish.

Some standard SCFT studies[75–77] reported finite size of free energy gaps and predicted that the surface-perpendicular morphologies become favorable due to the surface-induced compatabilization. Those SCFT research studies use incompressible block copolymer melts, and the hard neutral walls are represented by gradually decreasing density profiles near the surfaces. Due to the gradual reduction in the density in the surface region, the interaction between A and B segments is reduced near the neutral wall. This energetic effect promotes the perpendicular morphology in which more A-B contacts exist near the surface compared to the parallel one, and this phenomenon is referred to as the negative line tension.[75–77] In our theory, a similar effect is found due to the finite-range interaction despite that a step function shaped density profile is adopted.

We would like to emphasize that the value of the free energy must be carefully interpreted. One may think that as N increases, the chain has more segments, and thus it has more entropy due to the increase in flexibility. As observed in Figs. 9(b)–9(d), however, the absolute value of the excess free energy increases as N increases. It is because the freely gyrating chain provides the reference point of the entropy or free energy, and we only measure the loss of entropy with respect to this state, which actually diverges as $N \to \infty$. It does not create any problem because the free energy difference is all that matters, and Fig. 9 clearly shows that the free energy gap actually converges to 0 in this limit.

The aforementioned surface energy behavior is not a special feature of the FJC model. As displayed in section B of the

supplementary material, the BS model exhibits similar behavior, and a minor difference is observed at small N. Regarding the difference between the $N-1$ bond and N bond models, the absolute value of the excess free energy is higher for the N bond model because it has one more bond and each bond contributes a certain amount of entropy loss by the neutral wall. Even though the difference is not so noticeable, the size of the gap was also slightly bigger for the N bond model, and this is more difficult to explain. We speculate that the $N-1$ bond model's tendency of the chain end density increase near the wall reported by Matsen and co-workers[41,42] may provide a slight advantage to the surface parallel phase which naturally accumulates more chain ends at both walls.

Before ending this section, let us briefly discuss the advantage of the pseudospectral method over the full spectral method. The full spectral method was originally developed to obtain the phase diagram of the inhomogeneous polymer system, and it is extremely powerful when the symmetry of the morphology and the corresponding basis functions are well known. However, when the domain or boundary shape is complicated, the basis functions are practically impossible to predict, and the adoption of the pseudospectral method becomes necessary. Also, for the extremely highly stretched systems we tested in Subsection VI A, it is known that the full spectral method eventually becomes inefficient because of the fast increase in required basis functions.

VII. DISCUSSION AND CONCLUSION

The discrete chain self-consistent field theory can be a useful tool for the study of the short polymer systems. In this paper, its full algebraic formulation is presented and the issues of numerical implementation are discussed. Since the high computational demands of the real space method limit its applicability to the higher dimensional system, we propose the efficient numerical techniques utilizing the pseudospectral method for solving the recursive equations of the partial partition function.

For the purpose of efficient adaptation of the pseudospectral method, we presented a new algebraic description of the discrete chain SCFT adopting half-segment propagation in the calculation of the partial partition function. We examined the pseudospectral strategy for the three-dimensional FJC model whose discrete version has a limitation in representing the Dirac delta shaped bond function. To overcome this troublesome issue, we employed sampling theory of the DTFT which provides an efficient method to calculate DCT of the cell-averaged FJC bond function. The successful implementation of the pseudospectral method for both FJC and BS models was verified, and we confirmed that the discrete chain SCFT can be an efficient numerical tool performing calculations as fast as the standard SCFT.

As a model system, we applied the discrete chain SCFT to the analysis of symmetric block copolymers, and the chain behavior in the lamellar morphology was investigated. By calculating lamellar periods and interfacial widths for various chain models, we found that the FJC model behaves more like the standard SCFT due to residual mixing effect resulting from the step-shaped bond function.

In the standard SCFT calculation, Dirichlet and Neumann boundary conditions are the natural choices to model the physical boundary, but the discrete chain SCFT opens up a new possibility of adopting the neutral boundary condition. Unlike the other boundary conditions, neutral wall boundary requires a subtle consideration since DST is not applicable in its pseudospectral implementation. For this special case, we proposed a very simple technique which extends the system boundary beyond the neutral wall to allow the convolution integral calculation using DCT. By combining the neutral boundary with the finite-range interaction model, we studied the block copolymer thin film system confined by hard walls and successfully demonstrated how the surface-perpendicular block copolymer lamellar phase becomes preferable to the surface-parallel one when both the top and bottom surfaces are neutralized.

One special advantage of the discrete chain SCFT is that infinitely many possible polymer chain models can be adopted by replacing the bond function $g(\mathbf{r})$. For example, lattice SCFT[32,33] has been one branch of the SCFT, and we can reproduce the standard lattice SCFT in the Cartesian coordinates by adopting the $N-1$ bond model and using the following bond function:

$$g(0,0,\pm a) = g(0,\pm a,0) = g(\pm a,0,0) = \frac{1}{6}, \tag{32a}$$

$$g(x,y,z) = 0 \qquad \text{otherwise} \tag{32b}$$

in a spatial grid discretized by a.

It is well known that mean-field theory becomes inaccurate for systems of polymers with low molecular weight, and thus the discrete chain SCFT has its limitation for the analysis of short polymer candidates for high χ material. However, it at least incorporates the effect of finite segment size and number in the mean field theory, which is difficult to distinguish from the pure fluctuation effect. This approach is also useful when comparing results of SCFT to other particle-based simulations which include the full fluctuation effect. A recently emerging polymer simulation method is the single chain in mean field (SCMF) simulation[81–83] which attempts to incorporate the fluctuation effect in the field theoretical calculation by performing explicit MC simulation of polymer chains under the quasi-instantaneously updated self-consistent field. Because of this, the SCMF simulation is usually considered as an intermediate approach between the field-based simulation and particle-based simulation. The SCMF simulation inevitably employs polymer chains with a finite number of segments, and its density calculation method using discrete grids is reminiscent of the finite-range interaction of the discrete chain SCFT. These facts imply that the discrete chain SCFT is an intermediate theoretical tool residing in between the standard SCFT and SCMF simulation. That is, in the limit of infinitely many chains, the fluctuation effect becomes negligible, and the SCMF simulation result should converge to that of the discrete chain SCFT with the same chain model. If we additionally take $N \to \infty$ limit, the discrete chain SCFT finally converges to the standard SCFT. This relation implies that discrete chain SCFT can provide insight to distinguish the effect of finite segment from the effect of fluctuation.

We also feel like to mention the potential pedagogical advantage of the discrete chain SCFT. The formulation of the standard SCFT involves functional integrals over all the possible polymer paths. Proportionality constants are often floating in the functional integral, and many students and researchers who first learn this theoretical tool have trouble following all the algebraic steps. On the

other hand, the discrete chain SCFT formalism is very clear and neat, and it does not involve any functional integrals over the chain paths. Because of this, it is conceptually easier and all the partition function calculations can be done rigorously without any hidden proportionality constants. In summary, the discrete chain SCFT can provide a good starting point for those who are eager to learn the statistical mechanical method in polymer physics, and the use of the pseudospectral method makes it a promising tool for the research of various polymeric systems.

SUPPLEMENTARY MATERIAL

See supplementary material for the supplemented algebraic derivations of the discrete chain SCFT and results of free energy comparison using the BS chain model.

ACKNOWLEDGMENTS

We are grateful to Mark Matsen for useful discussions. This research was supported by the Basic Science Research Program through the National Research Foundation of Korea (NRF) funded by the Ministry of Science, ICT and Future Planning (Grant Nos. 2014R1A2A1A11054430 and 2017R1A2B4012377). This research used high performance computing resources of the UNIST Supercomputing Center.

APPENDIX: CALCULATION OF FJC $\bar{g}_i$ USING SAMPLING THEORY OF DTFT

In this appendix, we explain how the cell-averaged g_i of the FJC model defined by Eq. (29) can be calculated using a few equations in the DTFT and the sampling theory. For simplicity, we demonstrate the one-dimensional version of the calculation in which our aim is to calculate

$$g_k \equiv \frac{1}{\Delta z}\int_{-\Delta z/2}^{\Delta z/2} g\left(k\Delta z - z'\right)dz'. \tag{A1}$$

We start by defining a continuous average function,

$$\bar{g}(z) \equiv \frac{1}{\Delta z}\int_{-\Delta z/2}^{\Delta z/2} g\left(z - z'\right)dz', \tag{A2}$$

which makes $\bar{g}(k\Delta z)$ as our target array g_k. Because $\bar{g}(z)$ is a convolution of $g(z)$ and a rectangular function which is defined as $\Pi(x) \equiv 1$ only when $|x| \le 1/2$,

$$\bar{g}(z) = \frac{1}{\Delta z}\int_{-\infty}^{\infty} g\left(z - z'\right)\Pi\left(\frac{z'}{\Delta z}\right)dz'. \tag{A3}$$

Using the convolution theorem, the Fourier transform of $\bar{g}(z)$ is calculated as

$$\tilde{\bar{g}}(\xi) = \tilde{g}(\xi)\mathrm{sinc}(\xi\Delta z) = \mathrm{sinc}(2\xi a)\mathrm{sinc}(\xi\Delta z), \tag{A4}$$

where the last equation uses the Fourier transform of the one-dimensional FJC bond function.

The DTFT of a generic function $f(z)$ sampled at interval Δz is

$$F(\xi) \equiv \Delta z \sum_{n=-\infty}^{\infty} f(n\Delta z)e^{-i2\pi\xi\Delta z n}, \tag{A5}$$

and it is a periodic summation of $\tilde{f}(\xi)$ which is a Fourier transform of $f(z)$,[84]

$$F(\xi) = \sum_{n=-\infty}^{\infty} \tilde{f}\left(\xi - \frac{n}{\Delta z}\right). \tag{A6}$$

When an even function $f(z)$ is defined at $-L_z < z < L_z$ and zero outside this region, we can relate the DTFT with the DCT by setting $\xi = k/2L_z$, where $L_z = K\Delta z$,

$$\begin{aligned}\frac{1}{2\Delta z}F\left(\frac{k}{2\,K\Delta z}\right) &= \frac{1}{2}\sum_{n=-\infty}^{\infty} f(n\Delta z)e^{-i\pi nk/K} \\ &= \sum_{n=0}^{K}{}' f(n\Delta z)\cos\left(\frac{\pi nk}{K}\right) = \tilde{f}_k.\end{aligned} \tag{A7}$$

Applying this relation to $\bar{g}(z)$ and using Eqs. (A4) and (A6),

$$\begin{aligned}\tilde{g}_k &= \frac{1}{2\Delta z}\bar{G}\left(\frac{k}{2L_z}\right) = \frac{1}{2\Delta z}\sum_{n=-\infty}^{\infty}\tilde{\bar{g}}\left(\frac{k}{2L_z} - \frac{n}{\Delta z}\right) \\ &= \frac{1}{2\Delta z}\sum_{n=-\infty}^{\infty}\mathrm{sinc}\left(a\frac{k-2n_zK}{L_z}\right)\mathrm{sinc}\left(\frac{k-2n_zK}{2K}\right).\end{aligned} \tag{A8}$$

It is straightforward to extend this result to the three-dimensional system to obtain Eq. (30).

REFERENCES

[1] S. Park, D. H. Lee, J. Xu, B. Kim, S. W. Hong, U. Jeong, T. Xu, and T. P. Russell, Science **323**, 1030 (2009).
[2] A. B. Djurišić, A. M. C. Ng, and X. Y. Chen, Prog. Quantum Electron. **34**, 191 (2010).
[3] Y. Shi, L. Peng, Y. Ding, Y. Zhao, and G. Yu, Chem. Soc. Rev. **44**, 6684 (2015).
[4] Z. Tang, C. He, H. Tian, J. Ding, B. S. Hsiao, B. Chu, and X. Chen, Prog. Polym. Sci. **60**, 86 (2016).
[5] F. S. Bates and G. H. Fredrickson, Annu. Rev. Phys. Chem. **41**, 525 (1990).
[6] F. S. Bates and G. H. Fredrickson, Phys. Today **52**(2), 32 (1999).
[7] M. W. Matsen, J. Phys.: Condens. Matter **14**, R21 (2002).
[8] M. W. Matsen, in *Soft Matter*, edited by G. Gompper and M. Schick (Wiley VCH, Weinheim, 2006), Vol. 1.
[9] Y.-B. Yang, Y. J. Choi, S. O. Kim, and J. U. Kim, Soft Matter **11**, 4496 (2015).
[10] P. G. de Gennes, *Scaling Concepts in Polymer Physics* (Cornell University Press, Ithaca; London, 1979).
[11] J.-L. Brédas, D. Beljonne, V. Coropceanu, and J. Cornil, Chem. Rev. **104**, 4971 (2004).
[12] B. K. Rao and M. L. Verma, Chem. Phys. Lett. **679**, 176 (2017).
[13] R. O. Agbaoye, P. O. Adebambo, J. O. Akinlami, T. A. Afolabi, S. Zh. Karazhanov, D. Ceresoli, and G. A. Adebayo, Comput. Mater. Sci. **139**, 234 (2017).
[14] F. W. Starr, T. B. Schrøder, and S. C. Glotzer, Macromolecules **35**, 4481 (2002).
[15] Y. Han and J. Elliott, Comput. Mater. Sci. **39**, 315 (2007).
[16] Q. Wei, Y. Wang, W. Chai, Y. Zhang, and X. Chen, Ceram. Int. **43**, 13702 (2017).
[17] W. Peng, R. Ranganathan, P. Keblinski, and R. Ozisik, Macromolecules **50**, 6293 (2017).
[18] A. C. F. Mendonça, F. Goujon, P. Malfreyt, and D. J. Tildesley, Phys. Chem. Chem. Phys. **18**, 6164 (2016).
[19] C. Greco, Y. Jiang, J. Z. Y. Chen, K. Kremer, and K. C. Daoulas, J. Chem. Phys. **145**, 184901 (2016).
[20] S. F. Edwards, Proc. Phys. Soc., London **85**, 613 (1965).
[21] G. H. Fredrickson, *The Equilibrium Theory of Inhomogeneous Polymers* (Oxford University Press, New York, 2006).
[22] J. U. Kim and M. W. Matsen, Phys. Rev. Lett. **102**, 078303 (2009).
[23] B. Vorselaars, J. U. Kim, T. L. Chantawansri, G. H. Fredrickson, and M. W. Matsen, Soft Matter **7**, 5128 (2011).

[24]M. W. Matsen and M. Schick, Phys. Rev. Lett. **72**, 2660 (1994).
[25]M. W. Matsen, Macromolecules **45**, 2161 (2012).
[26]S.-M. Park, X. Liang, B. D. Harteneck, T. E. Pick, N. Hiroshiba, Y. Wu, B. A. Helms, and D. L. Olynick, ACS Nano **5**, 8523 (2011).
[27]J. W. Jeong, W. I. Park, L.-M. Do, J.-H. Park, T.-H. Kim, G. Chae, and Y. S. Jung, Adv. Mater. **24**, 3526 (2012).
[28]J. G. Son, M. Son, K.-J. Moon, B. H. Lee, J.-M. Myoung, M. S. Strano, M.-H. Ham, and C. A. Ross, Adv. Mater. **25**, 4723 (2013).
[29]I. Y. Erukhimovich, A. Johner, and J. F. Joanny, Eur. Phys. J. E **27**, 435 (2008).
[30]M. W. Matsen, J. U. Kim, and A. E. Likhtman, Eur. Phys. J. E **29**, 107 (2009).
[31]S. Blaber, P. Mahmoudi, R. K. W. Spencer, and M. W. Matsen, J. Chem. Phys. **150**, 014904 (2019).
[32]J. M. H. M. Scheutjens and G. J. Fleer, J. Phys. Chem. **83**, 1619 (1979).
[33]J. M. H. M. Scheutjens and G. J. Fleer, J. Phys. Chem. **84**, 178 (1980).
[34]T. Cosgrove, T. Heath, B. van Lent, F. Leermakers, and J. Scheutjens, Macromolecules **20**, 1692 (1987).
[35]G. T. Pickett and A. C. Balazs, Macromolecules **30**, 3097 (1997).
[36]M. Deng, Y. Jiang, H. Liang, and J. Z. Y. Chen, Macromolecules **43**, 3455 (2010).
[37]Y. Jiang and J. Z. Y. Chen, Phys. Rev. Lett. **110**, 138305 (2013).
[38]S. M. Ross, *Introduction to Probability Models* (Academic Press, Amsterdam, 2010).
[39]H. Yamakawa, *Modern Theory of Polymer Solutions* (Harper & Row, New York, 1971).
[40]A. Y. Grosberg and A. R. Khokhlov, *Statistical Physics of Macromolecules* (AIP Press, New York, 1994).
[41]M. W. Matsen and P. Mahmoudi, Eur. Phys. J. E **37**, 78 (2014).
[42]P. Mahmoudi and M. W. Matsen, Eur. Phys. J. E **39**, 78 (2016).
[43]P. Mahmoudi and M. W. Matsen, Eur. Phys. J. E **40**, 85 (2017).
[44]D. Romeis, H. Merlitz, and J.-U. Sommer, J. Chem. Phys. **136**, 044903 (2012).
[45]M. W. Matsen, Macromolecules **45**, 8502 (2012).
[46]J. U. Kim, Y.-B. Yang, and W. B. Lee, Macromolecules **45**, 3263 (2012).
[47]E. Helfand, J. Chem. Phys. **62**, 999 (1975).
[48]F. Drolet and G. H. Fredrickson, Phys. Rev. Lett. **83**, 4317 (1999).
[49]F. Drolet and G. H. Fredrickson, Macromolecules **34**, 5317 (2001).
[50]G. H. Fredrickson, V. Ganesan, and F. Drolet, Macromolecules **35**, 16 (2002).
[51]P. Tang, F. Qiu, H. Zhang, and Y. Yang, Phys. Rev. E **72**, 016710 (2005).
[52]J. F. Li, J. Fan, H. D. Zhang, F. Qiu, P. Tang, and Y. L. Yang, Eur. Phys. J. E **20**, 449 (2006).
[53]J. U. Kim and M. W. Matsen, Macromolecules **41**, 246 (2008).
[54]J. U. Kim and M. W. Matsen, Soft Matter **5**, 2889 (2009).
[55]J. Li, H. Zhang, and F. Qiu, Eur. Phys. J. E **37**, 18 (2014).
[56]Y.-B. Yang, Y. M. Jeon, J. U. Kim, and J. Cho, Eur. Phys. J. E **35**, 86 (2012).
[57]D. Yong and J. U. Kim, Phys. Rev. E **96**, 063312 (2017).
[58]K. Ø. Rasmussen and G. Kalosakas, J. Polym. Sci., Part B: Polym. Phys. **40**, 1777 (2002).
[59]H. D. Ceniceros and G. H. Fredrickson, Multiscale Model. Simul. **2**, 452 (2004).
[60]E. W. Cochran, C. J. Garcia-Cervera, and G. H. Fredrickson, Macromolecules **39**, 2449 (2006).
[61]A. Ranjan, J. Qin, and D. C. Morse, Macromolecules **41**, 942 (2008).
[62]P. Stasiak and M. W. Matsen, Eur. Phys. J. E **34**, 110 (2011).
[63]D. Lee, M.-H. Kim, D. Bae, G. Jeon, M. Kim, J. Kwak, S. J. Park, J. U. Kim, and J. K. Kim, Macromolecules **47**, 3997 (2014).
[64]W. H. Press, B. P. Flannery, S. A. Teukolsky, and W. T. Vetterling, *Numerical Recipes: The Art of Scientific Computing* (Cambridge University Press, Cambridge, 2007).
[65]M. Frigo and S. G. Johnson, Proc. IEEE **93**, 216 (2005).
[66]Y.-B. Yang, S. J. Park, P. Kim, and J. U. Kim, Soft Matter **9**, 5624 (2013).
[67]S. Wu, *Polymer Interface and Adhesion* (CRC Press, New York, 1982).
[68]Y. Kim, D. Yong, W. Lee, S. Jo, H. Ahn, J. U. Kim, and D. Y. Ryu, Macromolecules **51**, 8550 (2018).
[69]P. Mansky, T. P. Russell, C. J. Hawker, J. Mays, D. C. Cook, and S. K. Satija, Phys. Rev. Lett. **79**, 237 (1997).
[70]E. Han, K. O. Stuen, M. Leolukman, C.-C. Liu, P. F. Nealey, and P. Gopalan, Macromolecules **42**, 4896 (2009).
[71]P. Mansky, Y. Liu, E. Huang, T. P. Russell, and C. Hawker, Science **275**, 1458 (1997).
[72]R. D. Peters, X. M. Yang, T. K. Kim, B. H. Sohn, and P. F. Nealey, Langmuir **16**, 4625 (2000).
[73]J. Y. Kim, B. H. Kim, J. O. Hwang, S.-J. Jeong, D. O. Shin, J. H. Mun, Y. J. Choi, H. M. Jin, and S. O. Kim, Adv. Mater. **25**, 1331 (2013).
[74]G. T. Pickett, T. A. Witten, and S. R. Nagel, Macromolecules **26**, 3194 (1993).
[75]D. Meng and Q. Wang, J. Chem. Phys. **126**, 234902 (2007).
[76]M. W. Matsen, J. Chem. Phys. **106**, 7781 (1997).
[77]T. Geisinger, M. Müller, and K. Binder, J. Chem. Phys. **111**, 5241 (1999).
[78]H.-Y. Chen and G. Fredrickson, J. Chem. Phys. **116**, 1137 (2002).
[79]W. H. Tang, Macromolecules **33**, 1370 (2000).
[80]S.-J. Jeong, H.-S. Moon, J. Shin, B. H. Kim, D. O. Shin, J. Y. Kim, Y.-H. Lee, J. U. Kim, and S. O. Kim, Nano Lett. **10**, 3500 (2010).
[81]K. C. Daoulas, M. Müller, J. J. de Pablo, P. F. Nealey, and G. D. Smith, Soft Matter **2**, 573 (2006).
[82]B. Steinmüller, M. Müller, K. R. Hambrecht, G. D. Smith, and D. Bedrov, Macromolecules **45**, 1107 (2012).
[83]L. Schneider and M. Müller, Comput. Phys. Commun. **235**, 463 (2019).
[84]A. V. Oppenheim, A. S. Willsky, and S. Hamid, *Signals and Systems*, 2nd ed. (Prentice-Hall, New York, 1996).